

2019-01-01

In Situ Selective Nitriding Using An Open Source Laser Powder Bed Fusion System

Andres Gerardo Navarro
University of Texas at El Paso

Follow this and additional works at: https://scholarworks.utep.edu/open_etd



Part of the [Mechanical Engineering Commons](#)

Recommended Citation

Navarro, Andres Gerardo, "In Situ Selective Nitriding Using An Open Source Laser Powder Bed Fusion System" (2019). *Open Access Theses & Dissertations*. 3011.
https://scholarworks.utep.edu/open_etd/3011

This is brought to you for free and open access by ScholarWorks@UTEP. It has been accepted for inclusion in Open Access Theses & Dissertations by an authorized administrator of ScholarWorks@UTEP. For more information, please contact lweber@utep.edu.

IN SITU SELECTIVE NITRIDING USING AN OPEN SOURCE LASER
POWDER BED FUSION SYSTEM

ANDRES GERARDO NAVARRO

Master's Program in Mechanical Engineering

APPROVED:

Ryan Wicker, Ph.D., Chair

Francisco Medina, Ph.D.

Amit Lopes, Ph.D.

Cesar Terrazas, Ph.D.

Stephen Crites, Ph.D.
Dean of the Graduate School

Copyright ©

by

Andres Gerardo Navarro

2019

This Thesis is Dedicated to My Family Who Have Supported and Encouraged Me to Achieve
My Academic Goals and Pursue My Education Through Hard Work and Determination.

IN SITU SELECTIVE NITRIDING USING AN OPEN SOURCE LASER
POWDER BED FUSION SYSTEM

by

ANDRES GERARDO NAVARRO, B.S.M.E

THESIS

Presented to the Faculty of the Graduate School of

The University of Texas at El Paso

in Partial Fulfillment

of the Requirements

for the Degree of

MASTER OF SCIENCE

Department of Mechanical Engineering

THE UNIVERSITY OF TEXAS AT EL PASO

August 2019

ACKNOWLEDGEMENTS

I am incredibly grateful to Dr. Ryan Wicker, director of the W.M. Keck Center for 3D Innovation (Keck Center), for having provided me the opportunity to learn and grow through doing research as a graduate student. His support and knowledge have allowed me to develop as an engineer in the world of Additive Manufacturing and his critiques and advice have helped me grow as a professional. My supervisor Mr. Philip Morton, Applications Manager at the Keck Center has provided me with feedback and guidance through my time at the Keck Center and has mentored me and pushed me to improve my way of thinking and working to constantly improve.

Over the course of my time doing research certain individuals have been imperative in my development. Dr. Cesar Terrazas has provided me with an abundance of knowledge about the world of Additive Manufacturing and his critiques and comments have allowed me to improve as a researcher and helped to improve my technical writing abilities. Mr. Alfonso Fernandez and Mr. Hunter Taylor who have worked alongside me in my research and have helped me perform experiments or sample analysis.

Support for this project was provided through the MSI STEM Research & Development Consortium sponsored by the U.S. Army via cooperative agreement #W911SR-14-2-0001

PROJECT NUMBER 0025

ABSTRACT

Over the years thermochemical surface engineering techniques have been used to increase the mechanical properties of components for a variety of mechanical uses. Among these surface engineering techniques, nitriding is one of the most common practices. Conventional forms of nitriding limit the locations to surfaces, limiting applications to simple coatings. The aim throughout this research was to increase the uses of nitriding by applying the techniques to additive manufacturing (AM) technologies.

AM technologies provide the opportunity for surface coating methods to be utilized within the layer by layer fabrication method and for nitride regions within solid substrates increasing internal material properties and forming Ti/TiN metal matrix composites. Of the AM technologies available for use, laser powder bed fusion (LPBF) provides a fabrication process with the correct thermal energy source and processing environment to allow for the nitriding of substrates during their fabrication process to be possible. This project utilizes an AconityONE open source LPBF system with custom laser parameter settings to fabricate and nitride Ti-6Al-4V substrates. Laser nitriding parameters were developed by nitriding wrought grade 2 titanium, wrought grade 5 Ti-6Al-4V, and substrates fabricated from Grade 23 Ti-6Al-4V powder.

Initial laser nitriding parameters were conducted on wrought titanium samples by varying laser power and scanning speed. Nitrided regions of the samples demonstrated a more consistent nitride layer for laser parameters utilizing slower scanning speeds when compared to those at much faster scanning speeds at the same laser power. Nitrided regions on the Grade 2 Ti substrates showed TiN dendrite formation with layer thicknesses averaging $\sim 50\text{-}100\mu\text{m}$ and a hardness of $1200\text{-}1800\text{ VHN}$. These nitrided regions were examined as surface nitrided layers as well as having a single layer of Grade 23 Ti-6Al-4V powder melted atop the nitrided regions.

Similar nitriding parameters did not provide the same level of nitriding on Grade 5 substrates and additional laser parameters were taken in to consideration to improve nitriding results.

Modulated width (MW) or pulsed laser parameters were utilized to provide laser parameters to compare to the default continuous wave (CW) parameters. These MW laser parameters showed better initial signs of nitriding on the Grade 5 Ti-6Al-4V substrates by producing the golden surface color attributed to TiN that was not produced with the CW laser parameters. Various modifications to the laser parameters were such as changes to scanning speed, laser power, the defocus values of the laser beam, and varying hatch spacing between line scans were used in an attempt to better understand what the effects of individual parameters modifications had on the formation of the TiN layers.

Fabrication of substrates utilizing the Grade 23 Ti-6Al-4V powder was performed utilizing default titanium fabrication laser parameters. These parameters proved insufficient to cause nitriding but did produce a burning effect in a nitrogen environment. Nitriding was performed and examined on both the surface of the samples as well as in multi-nitride layer parts. These sandwich builds (i.e., embedding TiN sections between layers of Ti-6Al-4V) were utilized to evaluate the effects of single nitride layers within fabricated substrates and their effects on the sample's integrity. Through the use of both CW and MW laser parameters it was shown that CW laser parameters were successfully able to nitride the samples showing both a golden surface finish as well as dendrites throughout the microstructure while MW parameters did not show either of these characteristics. A correlation was shown where the more focused the laser beam was by having the defocus value closer to 0, the deeper the melt pool depth will be into the substrate. The depth for both CW and MW laser parameters was similar for the melt pool depth, however the heat affected zone depth varied more significantly as the CW parameters

showed a heat affected zone $\sim 100\mu\text{m}$ deeper than the MW. Microhardness measurements of the sandwich parts was lower than expected ranging from 600-1300VHN, however the increase in hardness from the base material by 200-800VHN showed large improvement.

Through this research it was demonstrated that nitriding can be integrated into the fabrication of titanium parts through the use of open source laser powder bed fusion systems. Multiple laser outputs can be utilized to achieve nitriding, however CW laser parameters with lower scanning speeds produced the best results thus far.

CONTENTS

Acknowledgements.....	v
Abstract.....	vi
Contents	ix
List of Tables	xi
List of Figures	xii
Chapter 1: Introduction.....	1
Background.....	1
1.2 Objective.....	3
1.3 Motivation.....	3
1.4 Thesis Outline	4
Chapter 2: Literature Review.....	5
2.1 Additive Manufacturing.....	5
2.2 Nitriding.....	8
Chapter 3: Experimental Methodology.....	13
3.1 Laser powder-bed fusion Setup and production	13
3.2 Laser Nitriding.....	17
3.3 Post processing after build.....	17
3.4 Sample Preparation	18
3.5 Microstructure and Microhardness Analysis	20
3.6 Surface Nitriding Experiments	21
Chapter 4: Results.....	33
4.1 Preliminary Grade 2 titanium substrate Nitriding.....	33
4.2 Preliminary Grade 5 substrate nitriding.....	34
4.3 Second Grade 5 Titanium Substrate Nitriding-Defocus Testing	35
4.4 Grade 2 titanium substrate nitriding Sandwiching Experiment.....	37
4.5 Grade 5 Ti-6Al-4V Pulsed Laser Experiment	43
4.6 Initial Grade 23 Ti-6Al-4V Powder Build Surface Nitriding	46
4.7 Sandwich experiment 1.....	57
4.8 Sandwich experiment 2.....	63

4.9 Ti-6Al-4V/TiN Parameter Refinement Test	64
Chapter 5: Conclusion.....	70
5.1 Discussion	70
5.2 Conclusion	73
5.3 Future Work	74
References.....	75
Vita	77

LIST OF TABLES

Table 4.1 Corresponding laser parameters for each sample in Figure 4.1	34
Table 4.2 Corresponding laser parameters for samples in Figure 4.2	35
Table 4.3 Corresponding laser parameter settings for Figure 4.3	37
Table 4.5.1 Lists corresponding laser parameters for samples in Figure 4.9	45
Table 4.7 Lists the laser parameters used in Figure 4.20	58
Table 4.8 Average micro-hardness values obtained from horizontal regions in the cross-section corresponding to images shown in Figure 4.23	62

LIST OF FIGURES

Figure 2.1 Basic setup of an SLM system (CustonPart.net, 2012).....	7
Figure 2.2 A) melt pool with a low thermal diffusivity and high Prandtl number; B) Melt pool with a higher melting temperature and high Marangoni number.....	12
Figure 3.1 AconityONE Laser Powder bed Fusion System.....	14
Figure 3.2 Internal view of the AconityONE build chamber A) Powder Supply B) Build platform.....	15
Figure 3.3 Relative positions of raking system, powder bed platform, and build platform.....	15
Figure 3.4 A) Displays the position of the squares nitrated on the substrate. B) Shows the corresponding laser parameters for each square.....	22
Figure 3.5 A) Displays the position of designs files used to test defocus settings. B) Depicts the constant laser parameter used as well as corresponding defocus values for each sample.....	23
Figure 3.6 A) The orientation and position of substrates used during the substrate nitriding sandwich experiment. B) Lists the parameters for both the nitriding process as well as the melting of Ti-6Al-4V powder layer.....	25
Figure 3.7 A) Displays the layout of nitrated cubes for the pulsed Ti-6Al-4V experiment. B) Details the 2 laser parameter sets used for the experiment. C) Lists the hatch spacing for each row as well as any changes made per sample.....	27
Figure 3.8 A) Demonstrates the locations of all cubes during the fabrication and nitriding process. B) Lists all parameters sets utilized for fabrication as well as base nitriding parameters. C) Lists the defocus values for each individual cube.....	28
Figure 3.9 A) Demonstrates the locations of all cubes during the fabrication and nitriding process. B) Lists all parameters sets utilized for fabrication as well as base nitriding parameters.....	30
Figure 3.10 A) Demonstrates the locations of all cubes during the fabrication and nitriding process. B) Lists all parameters sets utilized during fabrication and nitriding with all variables that were modified.....	32
Figure 4.1 Resulting nitriding layer produced utilizing initial laser nitriding parameters by changing laser power and scanning speed.....	33

Figure 4.2 A) Resulting nitriding layer produced utilizing laser nitriding parameters by changing laser power and scanning speed.....	35
Figure 4.3 Resulting nitriding layer produced utilizing laser nitriding parameters by changing laser power, defocus, and scanning speed.....	36
Figure 4.4 A) Depicts the samples post surface nitriding. B) Depicts samples after additional powder fusion has been performed on top of the nitrided surface.....	38
Figure 4.5 A zoomed in image at 20x magnification on an optical microscope with an added line to help separate the nitrided zone from the unaffected base substrate and the fused Ti-6Al-4V powder layer.....	39
Figure 4.6 Demonstrates different sections of the dendrites within the TiN microstructure. A) Contains areas of higher dendrite concentration at 100X magnification circled in blue. B&C) show the more distributed view of dendrites within the microstructure at 100X magnification. D) A slightly zoomed out image at 50X magnification with an overall view of the TiN layer as well as the transition from the base Grade 2 substrate.....	40
Figure 4.7 A) Highlights a large dendrite concentration ~50µm in length as a point of increased material hardness among the surrounding nitrided area at 100X magnification. B) Demonstrates a more evenly distributed dendrite microstructure with larger individual dendrites at 100X magnification. C&D) Provide an overview of the interactions between the sample materials along the cross-section surface. The interaction in the middle of the nitride layer can be seen in (C), while the farthest edge of the nitride can be seen in (D).....	41
Figure 4.8 A) Displays the micro-indentations performed on the substrates across three materials along a single axis. B) Displays the individual, and average hardness measurements taken from the micro-indentations on two separate samples; 1 and 2 from Figure 4.5.....	43
Figure 4.9 A) Displays the nitrided Grade 5 substrate after nitriding utilizing a pulsed laser configuration. B) Displays the corresponding sample setup used for the pulsed laser nitriding.....	44
Figure 4.10 Plots the data collected from measuring the width of single pass laser scans on all samples based on laser parameter and standard deviation for each hatch spacing...	45
Figure 4.11 A) Shows the orientation for samples used during experiment setup. B) Displays the overall results post nitriding.....	46

Figure 4.12 A) Depicts two laser scans. The difference in shape is due to the pulses not being parallel and only the edge of the let pool on the left being shown on the cross-section and not at its deepest penetration. B) Shows a more detailed view of a melt pool as well as the outline of the heat affected zone. C) Shows an enlarged view of the melt pool displaying the microstructure as well as some flow within the melt pool.....	48
Figure 4.13 A) Displays the nitrified area at 10X magnification. The dotted red line lies on the border of the heat affected zone. B) Shows a different melt pool of the nitrified region at 10X magnification.....	49
Figure 4.14 A) Displays the nitrified area at 20X magnification. The dotted red line lies on the border of the heat affected zone. B) Shows the nitrified region at 20X magnification where dendrites can be seen and is one of the two observed melt pool shapes. C) Displays the nitrified area at 20X magnification and depicts a different melt pool shape.....	50
Figure 4.15 A) Overview of melt pools in the cross section. B) A magnified view of a swirled melt pool pattern demonstrating flow.....	52
Figure 4.16 A) Overview of melt pools in the cross section. B) A magnified view of a swirled melt pool pattern demonstrating flow.....	53
Figure 4.17 A) Pulsed laser parameters at 0mm defocus. B) Pulsed laser parameters at -10mm defocus. C) Pulsed laser parameters at +10mm defocus. D CW laser parameters at -10mm defocus. E) CW laser parameters at +10mm defocus.....	55
Figure 4.18 Plot comparing melt pool depth to defocus values with the standard deviation for each sample.....	56
Figure 4.19 Plot comparing heat affected zone depth to defocus compared to the standard deviation.....	57
Figure 4.20 Depicts the orientation of samples arranged for the initial multi-layer nitride build with parameters run for each.....	58
Figure 4.21 A) Shows a wide show of the nitride layer with multiple laser scans. B) Demonstrates a connecting behavior between melt pools. C) A magnified image for inspection of the microstructure in a melt pool.....	60
Figure 4.22 shows images taken from 2 microscopes at 10X magnification of a crack growth stemming from the nitride layer.....	61
Figure 4.23 A) The highest micro-hardness value measured in the nitrified regions. B) A medium value measured in the nitrified regions. C) A lower hardness value measured in the nitrified region.....	63

Figure 4.24 A) Displays the setup of the samples. B) The view of the outer defects immediately after fabrication. C) Top view taken post nitriding before the continuation of the fabrication process. D) Parameters used during the fabrication and nitriding.....	64
Figure 4.25 A) Depicts the setup utilized for the samples as well as the rake and gas flow directions. B) Demonstrates the laser parameter settings for all samples.....	65
Figure 4.26 Samples maintained a constant laser power with varying scanning speeds and defocus levels.....	66
Figure 4.27 Samples maintained a constant power level and scanning speed with varying defocus causing variable overlap percentages.....	67
Figure 4.28 Samples contained varying laser power and scanning speed with consistent spot size and no overlap.....	68

CHAPTER 1: INTRODUCTION

BACKGROUND

Titanium and its alloys are extremely valuable materials in a variety of industries due to their desirable properties. High strength to weight ratio, high corrosion and heat resistance chief among them (Ani Zhecheva, 2004). Due to titanium's high strength to weight properties, it is used in a wide variety of applications such as the automotive and aerospace structural components, as well as a variety of medical applications such as implants and medical tools (Vojislav Petrovic, 2012). Although titanium has characteristics making it suitable for demanding applications, it is still possible to enhance some properties using surface manipulation techniques. For example, nitriding is the most common method of surface manipulation for titanium alloys and is used to increase surface hardness, wear resistance, and corrosion resistance (E. Gyorgy, 2002). Nitriding is the process in which a titanium substrate is exposed to a nitrogen rich environment and thermal energy, applied through a variety of sources, is used to bond nitrogen from the environment with a titanium substrate to form titanium nitride (Chi-Wai Chan S. L.-H.-C., 2015). Some common nitriding methods are gas nitriding, laser nitriding, plasma/ion nitriding, and liquid/salt bath nitriding. The resulting material is a metallic titanium core with a thin titanium nitride layer coating the area that was exposed to the thermal energy. Due to the current nitriding methods used, typical titanium nitrided components have a thin coating of $\sim 5\mu\text{m}$ in depth (Pye, 2003). Current nitriding techniques allow for the augmentation of certain characteristics in a substrate however, the benefits of nitriding are restricted to surface applications of fully dense parts and are not able to influence any internal characteristics (Pye, 2003). For this reason, Additive Manufacturing, specifically laser powder bed fusion, will be utilized in an attempt to integrate surface nitriding methods to create Ti-6Al-4V/TiN metal matrix composites.

Additive Manufacturing (AM), also referred to as rapid prototyping or 3D printing, is a fabrication process in which components are built in a layer by layer fashion. AM technologies use Computer Aided Design (CAD) software, such as Fusion 360(Autodesk, CA, USA), Inventor (Autodesk, CA, USA), or SolidWorks (Dassault Systems, MA, USA), to design part models which are then prepared in slicing software. Slicing software such as Magics (Materialise, Belgium, Germany) and NETFABB(Autodesk, CA, USA) convert the files to a format that can be processed by AM printers and assign parameters which the printers follow during the fabrication process (Kaufui V. Wong, 2012). The methods and materials vary depending on the AM technology being utilized; however, all AM technologies fabricate parts in a layer by layer method according to the parameters and specifications provided by the prepared software files. Post processing is required for parts upon completion. Post processing may include the removal of support structures used during fabrication, or being processed with equipment to section substrates and treat them to increase part strength or reduce internal stresses (Kaufui V. Wong, 2012).

Nitriding is a thermo-chemical coating method that is applied to metal components after they have been fabricated. These coatings are generally described as a thin coating not exceeding 10 μ m in depth (S. Fare, 2012). AM technologies, specifically laser based additive manufacturing, offers an environment where in situ nitriding can be performed during the fabrication process, increasing the ways the nitriding process can be applied by enabling internal nitriding and nitriding of regions that might otherwise prove inaccessible. Although typical laser powder bed fusion (LPBF) systems utilize an argon environment when working with Ti-6Al-4V, nitrogen gas was used to enable the system selectively form nitrides on the exposed surface of the fabricated substrate. This allows for nitriding to be utilized to form internal complex nitride structures. The improvement of this process is aimed to create an environment where titanium fabrication and

nitriding can be performed in an efficient process where complex parts can be fabricated with any desired nitride structure within the substrate geometry while not significantly increasing the fabrication time or increased waste of resources.

1.2 OBJECTIVE

The extremely valuable increase in material properties, such as surface hardness, corrosion and wear resistance, as well as aesthetic pleasing look has made titanium nitride a highly used material in a variety of industries. The objective of this research was to develop a process to form Ti-6Al-4V/TiN metal matrix composites with the use of laser powder bed fusion systems. These metal matrix composites aim to incorporate titanium nitride as part of the internal structure of the matrices as well as using it to intentionally reinforce titanium components fabricated through the use of laser additive manufacturing methods.

1.3 MOTIVATION

Integration of laser nitriding techniques into AM techniques, specifically LPBF, aims to fabricate tailored Ti-6Al-4V/TiN metal matrix composites with increased physical properties such as increased hardness in designated regions due to the selective formation of nitrides. The selective nature of the process allows for increased precision as well as better manipulation of properties within the metal matrices. These traits can become useful in industries where nitriding is already used by their ability to display multiple material properties in designated regions within a part's structure. Tools used for manufacturing and medical purposes can benefit from increased hardness in the form of better edge retention, as well as increasing the wear resistance of load regions in components, internal and external, while retaining flexibility and reduction of weight in sections of components where nitriding is not necessary. Increased control over nitriding can improve equipment for military usage increasing the life and performance of tools and weapons in extreme environments where reliability is imperative and replacement components are not abundant.

1.4 THESIS OUTLINE

The following thesis has been organized into 5 chapters. The current chapter (Chapter 1) has provided general background, motivation, objective and a general outline of the thesis. Chapter 2 serves as a literature review to provide background on the specific additive manufacturing methods utilized for this research and an in depth look at currently used nitriding methods. Chapter 3 will discuss the methodology that was used to nitride, fabricate components, and methods used to characterize the metal matrix composite articles. Chapter 4 will discuss the results of all experiments and the associated significant findings. Chapter 5 will conclude the work, discuss potential uses of this nitriding method, and outline future work to continue the research.

CHAPTER 2: LITERATURE REVIEW

2.1 ADDITIVE MANUFACTURING

Additive Manufacturing (AM) is a manufacturing method in which components are built in a layer by layer method from a computer-generated file. This type of manufacturing can be narrowed down to 7 process categories: powder bed fusion, directed energy deposition, material extrusion, material jetting, binder jetting, sheet lamination, and vat-photopolymerization (ASTM F2792-10, 2010). These AM technologies can produce components out of metals, polymers, ceramics, as well as composite materials. AM follows a set of steps common to all 7 categories which are: 1) Computer Aided Design modeling, 2) conversion to STL/STEP through software, 3) slicing of STL or STEP files along with their support structure, 4) toolpath generation for machine processing, 5) setup of the additive manufacturing machine, 6) layer by layer fabrication of the component, and 7) post processing of completed part. AM was used for the fabrication of models and prototype parts in the early years (Kaufui V. Wong, 2012). These parts were utilized to help engineers test components before fabricating end use parts. AM allows for benefits over conventional manufacturing techniques such as higher amounts of geometric freedom, faster production time, reduced development cost, and less material waste. The fabrication process utilized through AM technology does not require the use of molds or tooling allowing for faster time to market and reduced cost during low volume production. The design flexibility also allows for little to no change in cost from changes in design or fabrication parameter changes (Vojislav Petrovic, 2012). The additive nature of the technology reduces wasted material when compared to conventional subtractive manufacturing by as much as 40% during production. Additional material used during the processing such as metal powder, resin, or plastic, can be recycled and reused further reducing material waste (Vojislav Petrovic, 2012).

2.1.1 METAL BASED ADDITIVE MANUFACTURING

Metal additive manufacturing is primarily focused around three AM process categories, powder bed fusion (PBF), binder jetting, and directed energy deposition (DED). Two process categories, PBF and DED, utilize a thermal energy source, either laser or electron beam, to fabricate components (Valmik Bhavar, 2016). DED utilizes an energy source to provide the necessary thermal energy for processing of material. The thermal energy source creates a melt pool into which material is fed to build up material in that region. DED utilizes both powder and wire feedstock material. Commercially available powder feed processes are laser engineered net shaping (LENS), direct metal deposition (DMD), whereas processes that use wire feedstock are electron beam free form fabrication (EBFFF), and other arc-based technology (Valmik Bhavar, 2016). Within PBF there are two main sub categories, selective laser sintering/melting (SLS/SLM) and electron beam melting (EBM). Shielding gases are utilized for all laser base processes, while vacuum is used for electron beam processes to prevent oxidation of the metals.

2.1.2 POWDER BED FUSION

In PBF, an energy source is used to consolidate and melt metal powder, in a layer by layer fashion. Energy produced by either lasers or electron beams is used to selectively melt the powder in a layer by layer method according to the sliced STL file (Valmik Bhavar, 2016). After each consecutive layer, the build platform is lowered and the powder for the next layer provided from a secondary piston driven reservoir. A recoater mechanism, a rake or roller system, coats the building platform with another layer of powder and the process is repeated until the component has been completed (Valmik Bhavar, 2016). The time required to finish fabrication of components is mainly dependent on the size or number of components being fabricated as larger component or higher quantity of parts will extend the build time. Fabrication times will change based on the machine being used during the fabrication process as chamber size varies from machine to machine

and fabrication time per layer may vary. The technology used may also have an impact on fabrication time. For example SLM provides a higher level of accuracy and surface finish than DED and EBM but has longer production times than the two technologies (Valmik Bhavar, 2016).

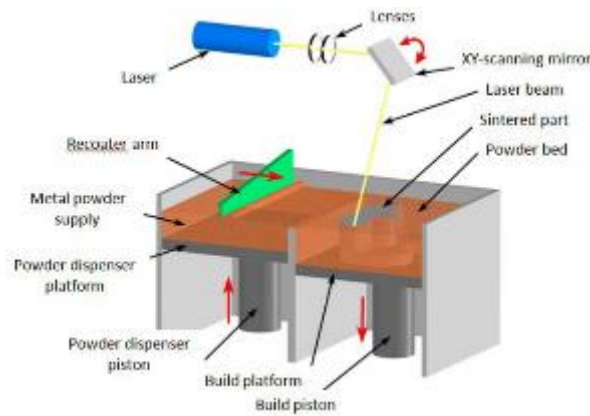


Figure 2.1 Basic setup of an SLM system (CustonPart.net, 2012)

SLM, like all AM technologies comes with limitations and common defects. Porosity and surface roughness are common among all seven forms of AM. Defects can be caused by material properties such as high diffusion of oxygen into metal powders during storage or parts during fabrication and conditions that could influence defects such as residual thermal stresses are especially common in metal-based AM. Some materials used in LPBF are prone to oxidation due to their high affinity for oxygen. The oxidation is minimized by processing all powder in inert environments as well as all fabrication environments requiring extremely low oxygen levels (Shunyu Liu, 2019). Residual thermal stresses are also common in SLM due to the use of high localized heating and cooling rates from the laser beams during processing. Heating of the build plate and controlling the direction in which the component is scanned during fabrication can help to more evenly distribute the thermal load and reduce the likelihood of cracking and warping due to the residual stresses. (Shunyu Liu, 2019). Post processing methods such as annealing are

commonly used to increase yield strength at the expense of reducing ultimate tensile strength, and to reduce stresses within components before they are used. Although SLM can create near full density components under optimal processing conditions, factors such as uneven powder distribution, or impurities in the powder can cause porosity or other defects within components. Hot Isostatic Pressing (HIP) can be used as a post process, to correct some of these defects such as reducing porosity and densifying parts (Shunyu Liu, 2019).

2.2 NITRIDING

Nitriding is a form of thermochemical surface engineering, and the most commonly used technique in increasing surface properties such as hardness and wear resistance for titanium alloys (Yang, 2012). Developed in the early 1900's, nitriding has been adopted by a variety of industries including the automotive, aerospace, medical, and energy production (Pye, 2003). Properties that benefit from the bonding of nitrogen atoms into titanium substrates include surface hardness, wear resistance, corrosion resistance, and heat resistance (Yang, 2012). The process of bonding nitrogen atoms into a substrate to increase properties can be performed in two ways. First, using deposition techniques, where a coating is deposited over the substrates surface in order to treat it. The other is diffusional techniques where nitrogen is diffused into a substrate using chemical diffusion or heat and time (Deepak, 2015). Examples of deposition techniques include physical vapor deposition (PVD) and chemical vapor deposition (CVD), while processes such as laser or gas nitriding are considered a diffusional technique (Deepak, 2015).

There are four major diffusion categories of nitriding that are typically utilized; liquid salt bath nitriding, plasma/ion nitriding, gas nitriding, and laser nitriding (Pye, 2003). Nitriding is possible when nitrogen atoms are introduced to a titanium substrate surface at temperatures in excess of the material's recrystallization temperature (Deepak, 2015). The excessive heating in the

nitrogen rich environment causes the material to undergo a chemical change in which the TiN intermetallic is formed. This process can also occur in nitrogen rich environments but occurs at a slower rate due to lack of stimulus from heat. Nitriding for materials such as titanium is performed in environments with an abundance of nitrogen while limiting the oxygen to prevent formation of TiO₂ (Deepak, 2015). Pure nitrogen gas, ammonia, and nitrogen-argon mixtures can be used to ensure proper nitriding conditions. The resulting surface engineering results in a top layer of TiN and a layer of Ti₂N to form directly beneath it (Deepak, 2015).

2.2.1 NITRIDING TECHNIQUES

Salt bath nitriding relies on the decomposition of cyanide within the molten salt to release nitrogen which then diffuses into the substrate and is not generally used compared to other methods (Pye, 2003). Plasma nitriding offers higher levels of control of the nitride phase formation and the depth at which the nitride forms. The surface treatment requires high ionizing energy from special equipment such as cold-wall or hot-wall nitriding equipment. Ion beam nitriding makes use of the high energy spectrum unlike plasma nitriding which occupies the lower energy spectrum. A plasma/ion beam is used in a nitrogen and argon environment to nitride substrates (A R Nassar, 2012). Gas nitriding is generally the easiest nitriding method available and is regularly used in engineering applications (Ani Zhecheva, 2004). Gas nitriding offers more flexibility as part geometry does not affect nitriding capabilities and special equipment is not required. However, high temperatures ranging from 650-1000°C are required for long periods of time for nitrides to form (Ani Zhecheva, 2004).

2.2.2 LASER NITRIDING

Laser nitriding, sometimes referred to as laser gas nitriding, diffuses nitrogen from the processing atmosphere into the substrate with the use of thermal energy provided by a laser system.

Laser nitriding offers precision nitriding and provides superb bonding between the nitrided layer and the substrate surface but is more likely to cause cracking (Chi-Wai Chan S. L.-H.-C., 2015). The two most commonly used lasers employed for nitriding are CO₂-gas lasers which are typically operated in a Continuous Wave (CW) mode and Yttrium Aluminum Garnet (YAG) lasers which are operated in both CW or pulsed wave (PW) (Filip, 2008). CO₂ lasers operate at a wavelength of 10.6μm while YAG lasers emit radiation with a wavelength of 1.064μm. The power for both laser types can range anywhere between 0.5W-5kW (Filip, 2008). CO₂ lasers are commonly used lasers for nitriding materials such as Ti-6Al-4V.

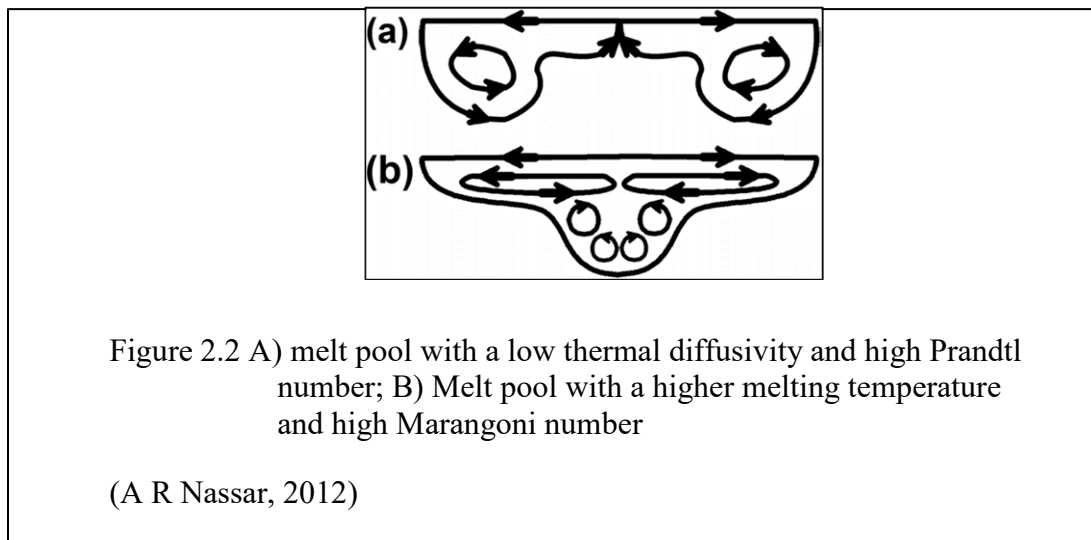
L. Xue and M. Islam conducted research on surface finish and cracking of nitrided Ti-6Al-4V with both CO₂ lasers and an Nd: YAG Laser (L. Xue, 2007). Laser parameters for the CO₂ were modified in terms of the lasers power and scanning speed. It was noted that higher laser power levels produced more even and smooth nitrided surfaces but also caused larger and a higher number of cracks to appear. As laser power was lowered, cracking decreased but the surface finish continuously worsened. Scanning speed did play a role in these results but laser power was observed to be the main contributing factor (L. Xue, 2007). The width of the melt zone was more directly affected by both factors as it was shown to widen with an increase in laser power or decrease in scanning speed or narrow with a decrease in laser power or increase in scanning speed (L. Xue, 2007). Xue concluded that a nitride layer that is both smooth and crack-free is not possible with the use of a CO₂ laser in CW. The same laser was operated in a pulsed method and increased in laser power throughout the testing. These tests led to a smoother surface and larger cracks until a certain level at which both surface finish and cracking would both continue to worsen. Due to the pulsed methods utilized by the laser, the width of the melt zone was mainly controlled by the length of the pulse width, so any change in scanning speed did not have as much of a significant

impact as it would during CW operation. It was noted that higher frequencies in the pulsed laser configuration caused some overlap between pulsed improving surface finish and reducing cracking up until a certain point. During testing 600-700Hz showed to be the threshold for these conditions (L. Xue, 2007). A pulsed method was used utilizing an Nd: YAG laser during the same sets of experiments and demonstrated smooth nitride layer formation with an increased laser pulse energy. Cracking did increase with the pulse energy levels but a ‘swirling’ pattern was noted in the melt pool most likely due to the material flow produced from the higher energy levels during the melting stage (L. Xue, 2007). L. Xue concluded that an Nd: YAG laser, although not as commonly utilized as CO₂ lasers, in a pulsed configuration was able to produce a more uniform, smooth and minimally cracked nitride layer in Ti-6Al-4V than a nitride layer produced utilizing a CO₂ laser.

The formation of nitride layers can vary depending on type of laser used as well as the output method of the laser. Lasers of different wavelengths as well as the laser energy output method, such as CW and MW, can affect the formation of nitrides. The individual laser parameters within the same laser types can also have a great impact in the success and quality of the nitriding process. Researchers such as Naofumi Ohutsu tested nitriding by comparing the hardness values produced by lasers of different wavelengths. They noticed that utilizing identical laser parameters, a deeper melt pool was formed with a smaller wavelength when compared to larger wavelength lasers (Naofumi Ohutsu, 2010).

During the nitriding process, due to heating and cooling of the substrate caused by the laser melting, different melt pool patterns can form. The convection currents developed within these melt pools determine the final geometry upon solidification of the melted material. Figure 2.2, demonstrates two such geometries that can be observed. The melt pool displayed in Figure 2.2 (A) is caused when melt pool geometry is mainly controlled by the flow of the convection currents. In

these instances, thermal diffusivity is found to be low and a high Prandtl number is present. Prandtl number is the non-dimensional value used to describe the relationship between momentum diffusivity and thermal diffusivity (A. Arora, 2008). These are caused when the surface tensions of the nitriding region increase due to a drop-in temperature. The hotter material flows to cooler regions of the substrate causing the material to move towards the edges. The cooler material flows downwards and back towards the center where it is reheated and travels towards the edges again (A. Arora, 2008). The melt pool pattern seen in Figure 2.2 (B) is caused by an increased melting temperature and larger Marangoni number. Marangoni number is the dimensionless variable used to describe the relationship between the thermal flow caused by a gradient in surface tension with thermal diffusion. This process occurs when the outward flowing material solidifies as it reaches the edges of the melt pool and the shallow upper currents cause multiple smaller flow currents in the opposite direction directly below (A. Arora, 2008).



CHAPTER 3: EXPERIMENTAL METHODOLOGY

3.1 LASER POWDER-BED FUSION SETUP AND PRODUCTION

Sample building and nitriding was performed using the AconityONE laser powder bed fusion (LPBF) system manufactured by Aconity3D (Aachen, Germany) shown in Figure 3.1. This system is equipped with a 1kW ytterbium-doped fiber laser with a wavelength of 1070nm capable of both Continuous Wave (CW) and Modulated Wave (MW) outputs. Regular fabrication in this system is conducted in a sealed chamber under an inert gas environment. For this project, a gas exchange process from Argon to Nitrogen was used in the experimental setups. This was done to prevent unwanted oxide formation from contact with oxygen from the surrounding air when the chamber is vented and prevent violent reactions due to the reactivity of titanium powder.

The machine setup began with cleaning the inside of the AconityONE by first vacuuming previous powder from the build chamber. Then, the build chamber was wiped using paper towels and isopropyl alcohol to remove unwanted dust, powder, or debris that may cause contamination of the feedstock powder. The next step consisted of powder preparation in which metallic powder was sieved using a pneumatic sieve with a gap size of 110 μ m to ensure powder size distribution (PSD) and to remove any debris or fused powder from the feedstock material. After the powder was sieved, the powder supply shown in Figure 3.2 (A) was lowered using the AconityONE interface and manually filled with the powder.

The build chamber was then closed and the raking system, seen in Figure 3.3, was used to distribute powder from the powder supply onto the build platform. This process was done by lowering the build platform and elevating the powder supply in small increments of ~2-10mm and repeatedly raking the powder into the build platform until the build plate has been completely covered with powder. The build platform was then raised in small increments ~0.25-1.5mm until

the build platform could be seen. This was done to ensure that the raking system was leveled and distributed an even layer of powder then the chamber was ready for purging. For substrates fabricated using metal powder, the chamber was purged using ultra high purity (UHP) argon gas provided by Airgas (El Paso TX, USA) at a rate of 13-16 l/min until oxygen levels in the chamber dropped below ≤ 500 ppm. Next, a fume extraction process, which activates a recirculation pump, was switched on to 70% capacity and the gas flow was reduced to 10 l/min until oxygen levels reached ≤ 300 ppm. Lastly, fume extraction was increased to 80-90% gas recirculation, the outlet valve was closed, the gas control pressure was set to ~ 30 mbar, and the gas flow was decreased to 4-8 l/min. These conditions allowed for a continuous flow within the chamber while limiting the amount of argon used. The building process proceeded once oxygen levels had dropped below 300 ppm. The purging of the system caused positive pressure inside the build chamber lifting the hood requiring the rake (which is fixed to the hood) to be re-leveled to ensure consistent powder spread. Small increments ~ 0.25 -1.5mm are used while re-leveling.



Figure 3.1 AconityONE Laser Powder bed Fusion System

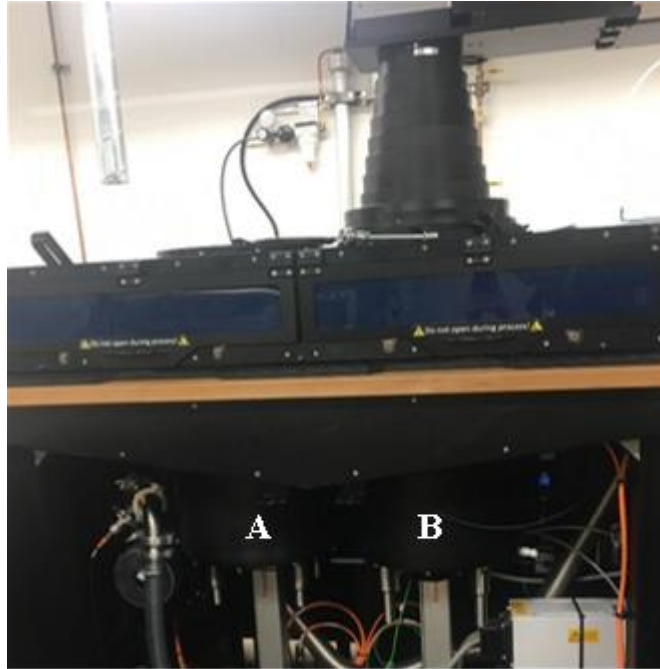


Figure 3.2 Internal view of the AconityONE build chamber
A) Powder Supply B) Build platform

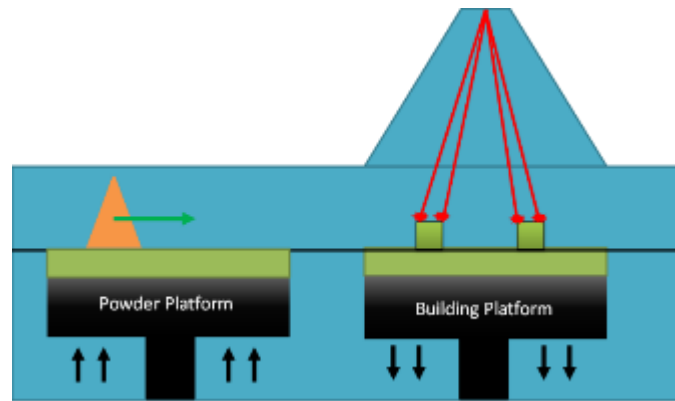


Figure 3.3 Relative positions of raking system,
powder bed platform, and build
platform

Fabrication files were generated using computer aided design software and pre-processing software. Part files were designed utilizing the Fusion360 computer aided design (CAD) software from Autodesk (Mill Valley, CA, USA). Once the components have been designed to the corresponding dimensions needed for that experiment, they were exported to a standard

tessellation language (STL) format. The files were then processed using the Magics software from Materialise (Belgium, Germany). Magics was used to orient parts, generate support structures, fix errors in the file such as holes, and set processing parameters that will be assigned to each part. Parameters input through software are hatch spacing, laser power, laser scanning speed, layer height, and angle rotation of laser beam during processing for all sections of a component, contour, volume, up skin, and down skin. Once files were completed, they were saved in a binary data format (.ILT) used for the AconityONE system. Files were loaded through the system interface and checked on the AconityONE system to ensure proper settings were transferred from software. Additional settings such as sample position and MW laser parameters are directly controlled from the AconityONE interface. The alignment laser was used to ensure sample placement was correct and allow for manual adjustments. Manual input of MW laser parameters was required and had to be aligned to match the correct sample setup.

3.1.1 LASER POWDER BED FUSION MATERIALS

The powder used in the builds throughout this work was Grade 23 Ti-6Al-4V metal powder sourced from LPW Technologies Inc. (Imperial, PA, USA). The powder had a spherical morphology with a particle size of 44-106 μ m according to the provider spec sheet. The titanium substrates used during the course of this project were wrought Grade 2 pure titanium which was the main substrate material used for initial nitriding testing and wrought Grade 5 Ti-6Al-4V procured from Armor Metals (El Paso, TX, USA). Both substrate materials were used to test nitriding parameters and study the effects of similar nitriding parameters on multiple materials. For nitriding performed on substrates fabricated using LPBF, as opposed to wrought substrates, the fabrication processes were performed under argon gas and stopped at 6mm.

3.2 LASER NITRIDING

During the nitriding setups, the substrates to be nitrided were centered on the build platform shown in Figure 3.2 (B) and visualized in Figure 3.3. During the fabrication process, a layer is selectively melted using the laser and recoated. This additional powder layer must be melted without being recoated in order to provide a powder-free, smooth surface for the nitriding process.

The nitriding process was performed using UHP Nitrogen gas provided by Airgas (El Paso TX, USA). The chamber was purged with nitrogen immediately before nitriding for the wrought and LPBF substrates. The chamber was purged with nitrogen at a flow rate of ~22 l/min. The gas flow rate undergoes a constant flow until the chamber reaches an oxygen level of <1000 ppm. The recirculation system would then be turned on at 70% capacity. while the system continued to purge. When oxygen levels had dropped to <300 ppm the recirculation system was increased to 85% and gas flow was lowered to ~10 l/min. At this point in the purging process the manual outlet valve was closed to reduce nitrogen consumption while oxygen levels drop further. While nitriding the substrates, the inlet gas flow was limited to ~5-8 l/min while internal pressure was set to 40mbar and recirculation as raised to 90%. The target range for nitriding was to maintain oxygen levels below 100 ppm, to ensure a nitrogen rich environment. Nitriding parameters utilized both CW and MW laser modes. All laser parameters for experiments performed utilized laser powers <400W.

CW laser parameters utilized for experiments included laser power, laser scanning speed, hatch spacing, and defocus values. Besides these parameters, for MW scanning additional parameters were used that included pulse width and frequency. Frequency is the number of laser pulses per second. Pulse width is the time which the laser is active during each pulse.

3.3 POST PROCESSING AFTER BUILD

After a component had been built and nitrided, it was removed from the build chamber. To carry out this process, the build chamber must first be allowed to purge out all of the inert gas used

during the fabrication process. Once the oxygen had risen to at least >2000 ppm, the chamber could be safely opened. Due to the high energy levels used by the laser for fabrication and/or nitriding, the substrates will have residual heat upon completion and should be allowed to cool before being removed from the chamber to reduce chances of unwanted oxides and nitrides forming from being exposed to air. No support structures were used in fabricated components for nitriding however parts were dusted off inside the AconityONE chamber to recover loose powder and minimize material waste.

3.4 SAMPLE PREPARATION

Samples that were fabricated and/or nitrided were prepared before characterization. This process involved cutting from the start plate, sectioning, mounting in resin, and finally grinding, polishing and etching before observation. Samples must first be cut off of their build platform. This was done utilizing an Hb 280B vertical bandsaw produced by Knuth (Chicago IL, USA) where the build plate was mounted in the vise and the saw was set to cut the samples within 3mm of the surface of the build platform. Components that were smaller or have already been separated from the build platform were sectioned using a Brilliant 220 compact precision wet abrasive cutter from ATM Mager Scientific (Mammelzen, Germany). Samples were cut using an abrasive alumina blade due to the high hardness of the titanium substrates as well as the selectively nitrided sections. The precision saw was run at 1800rpm with a feed rate of 2.2mm/min. A pulsed method was used to better cut the material, which cuts 1mm into the substrate, then backs out 2mm, then proceeds to make another 1mm cut. The pulsed method allows for better lubrication of the surface as well as decreasing the stress at a given time put onto the part.

Once samples had been properly sectioned, they were cleaned with isopropyl alcohol and dried off in order to be mounted. An OPAL 460.2 automatic hot mounting press (ATM Mager

Scientific, Mammelzen, Germany) was used to mount all samples. A powder release agent was applied to the bottom housing where samples were placed to ensure proper sample release after mounting. Sectioned samples were then positioned in the mounting press with the desired substrate face that is to be examined facing downwards. The platform was lowered and 2.5 scoops of black phenolic powder were poured into the chamber and evenly distributed. The mounting press was closed and set to 250°C and a pressure of 180 bar for a time limit of 3 minutes. The mounting press used an internal cooling system to cool after performing a mounting process taking ~3 minutes. Mounted samples were inspected to make sure all faces can be properly seen and are in the correct orientation. The back of each sample was then engraved for easy sample identification.

Mounted samples were polished utilizing a SAPHIR 560 procured from ATM, Mager Scientific (Mammelzen, Germany). The samples were mounted into the system holder and went through a 3-stage grinding and polishing process. Samples were first ground using a Rhaco grit P320 pad run with water under 35 N of distributed force at a speed of 300 rpm for both the sample mount and the grinding/polishing pad. The rotation of the samples and grinding/polishing pads are run in opposite directions. Grinding was performed in increments of 90 seconds before samples were examined. If samples displayed a planar face with no dents or deep scratches, then the samples were moved to the second stage. If more material must be removed, the grinding pad is replaced and the process is repeated until sufficient material has been removed to produce a scratch-free surface. Grinding pad replacement is necessary as the pads become ineffective after they have already been used for the 90 second process. The second stage of grinding makes use of an Aka-Allegran 3 diamond coated pad. The samples were run in a counter rotation movement at 150rpm and 25 N of distributed force for 3-5 minutes. A 6µm DiaMaxx diamond solution was added periodically to the grinding pad during the time limit to assist the process.

Once the samples had been evenly ground, they were moved to the polishing pad of the SAPHIR. An Aka-Chemal pad was used in combination with a solution composed of 0.2 μ m fumed silica suspended in an alkaline water-based solvent. Polishing was run under 150 rpms with a distributed load of 25N for a 3-5-minute period. When a mirror finish was achieved with no evident scratches or stains, the samples were etched using Krolls reagent consisting of 90ml of distilled water, 8ml of nitric acid, and 2ml of hydrofluoric acid. A swabbing method was used to distribute the etchant to the samples for 20 seconds, before being neutralized with isopropyl alcohol and then rinsed with a soap and water mixture.

3.5 MICROSTRUCTURE AND MICROHARDNESS ANALYSIS

3.5.1 MICROSTRUCTURE ANALYSIS

All samples were examined under an optical microscope. The optical microscope was used to find initial signs of successful nitriding in the form of dendrites. It was also used to examine the samples for defects such as porosity, cracking, or unusual melt pool morphology. The microscope used was an Olympus GX53 procured from Olympus Corp. (Center Valley, PA, USA). Samples were examined in nitrified areas to determine the presence of dendrites which would indicate increased nitrogen content, depth of the nitride layers, melt pool pattern, and defect such as cracks or delamination. Samples were given a preliminary scan looking for significant features such as dendrites and cracks at 2x magnification before focusing analysis on any particular area. When a feature was found, an image was taken of the area. Images were taken at each magnification and assigned a scale bar in μ m.

3.5.2 MICROHARDNESS ANALYSIS

Microhardness testing was performed on samples to determine hardness properties from nitrified regions. These values were compared to hardness values from surrounding regions on the

substrate. All testing was conducted with the use of a Duramin-A300 (Struer, Cleveland, Ohio, USA) with a load of 100gf load with a dwell time of 5 seconds. Microhardness measurements were taken using the Vickers hardness number (VHN). Measurements were taken across substrate cross-sections after they had been polished, etched, and analyzed under optical microscope and SEM. Measurements were taken from top to bottom of the interface surface starting from the left side of the substrate.

3.6 SURFACE NITRIDING EXPERIMENTS

3.6.1 PRELIMINARY GRADE 2 TITANIUM SUBSTRATE NITRIDING-PARAMETER TESTING

Preliminary surface nitriding was performed on a Grade 2 wrought titanium substrate. This test was focused on determining an ideal set of nitriding parameters using a grid of cubes, each with variable laser parameters. The substrates were cut from stock material to dimensions of 150mm x 40mm x 13mm for the Grade 2 titanium substrate utilizing the Hb 280B vertical bandsaw. Utilizing the guide beam in the AconityONE, the outer points of the cut substrates were matched with the location of the sample files and the substrate was adhered to the platform utilizing an adhesive tape to ensure alignment. The Grade 2 substrate was cleaned using isopropyl alcohol before and after being mounted to the build plate. The height of the substrate was measured and taken into account to ensure the top of the substrate was at the zero position in the focal plane of the laser before nitriding.

A matrix of three rows and seven columns of 10mm x 10mm squares was designed to test different parameters. The values assigned to each square as well as position can be seen in Figure 3.4. The parameters presented in Figure 3.4(B) are separated by square number where (P) represents the laser power assigned to the sample and (S) represents the scanning speed.

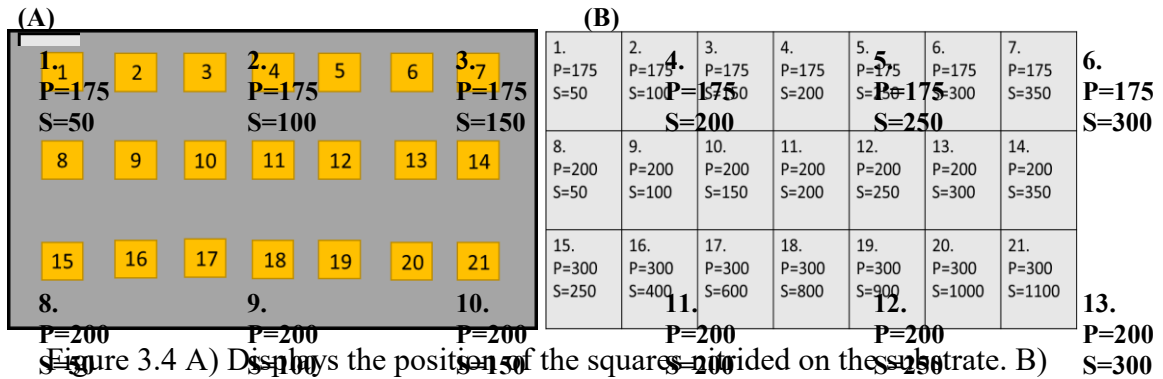


Figure 3.4 A) Displays the position of the squares provided on the substrate. B) Shows the corresponding laser parameters for each square.

Laser parameters were run in a continuous wave (CW) mode and varied based off of laser power and scan speed with laser power carrying from row to row and scan speed from column to column.

Each square geometry to be scanned was assigned a hatch spacing of 10μm with a 10mm stripe width. The file was then modified multiple times to provide 21 different laser parameters matching those displayed in Figure 3.4 (B). The completed ILT file was transferred to the AconityONE where each cube was individually moved to the positions seen in Figure 3.4 (A). For this experiment, nitriding was performed in a single scan before the substrate was removed from the chamber.

3.6.2 PRELIMINARY GRADE 5 TITANIUM SUBSTRATE NITRIDING-PARAMETER TESTING

Experiment 3.6.1 was reproduced utilizing a Ti-6Al-4V (Grade 5) substrate. Machine setup and nitriding setup follows steps outlined in sections 3.1 LPBF Setup and 3.2 Laser

Nitriding. The purpose of reproducing the initial parameter test experiment was to compare

nitriding results provided by identical nitriding conditions and laser parameters with a change in the substrate material. The Grade 5 substrate was cut from stock measuring 150mm x 70mm x

30mm. The substrate was aligned with assistance from the AconityONE guide beam and adhered to the build plate. Isopropyl alcohol was used to clean the substrate before closing the build

chamber. The parameters and part orientation used in this experiment was identical to that from 3.6.1.

3.6.3 GRADE 5 TITANIUM SUBSTRATE NITRIDING-DEFOCUS TESTING

Effects caused by the defocus of the laser beam were tested utilizing constant laser power and scanning speed while varying the defocus value for different samples. During this experiment a laser parameter set was held constant while a defocus variable was increased from one sample to the next. This experiment was conducted using a wrought Grade 5 Ti-6Al-4V substrate cut from stock measuring 150mm x 70mm x 30mm. Nitriding conditions were held constant as those described in section 3.2. Base laser parameters were held constant at a laser power of 175W and scan speed of 125mm/s while the laser defocus setting was varied between 13.5-19.5mm. Defocus values change the focal length of the laser modifying the laser beam spot size. This translates to different levels of overlap between the laser scan passes and a change in surface finish of the nitride may be seen. Higher amounts of overlap were shown to produce a smoother nitride surface.

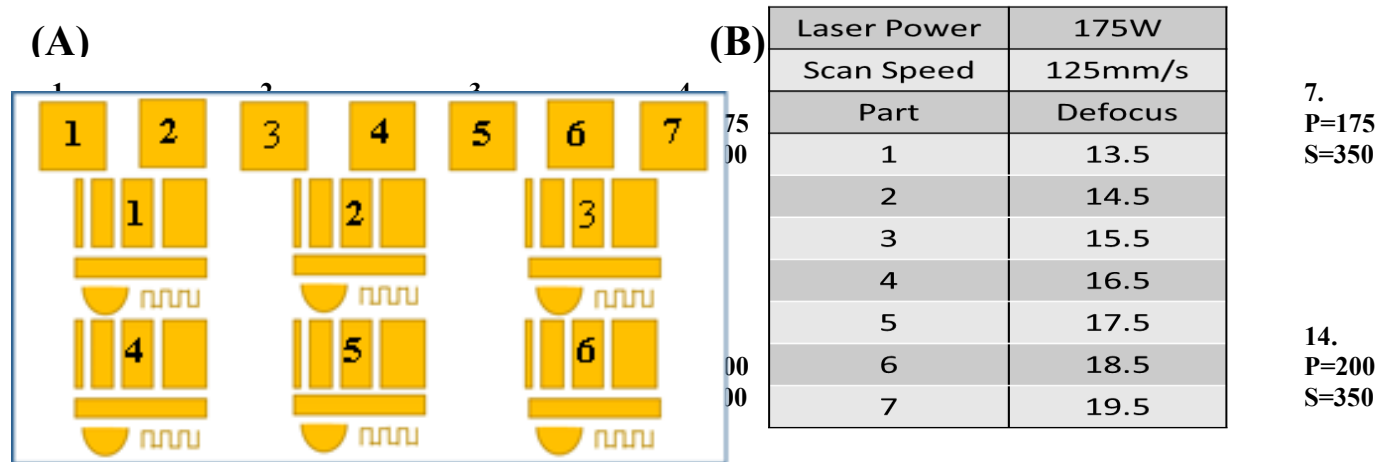


Figure 3.5 A) Displays the position of designs files used to test defocus settings. B) Depicts the constant laser parameter used as well as corresponding defocus values for each sample.

15. P=300 S=250 16. P=300 S=400 17. P=300 S=600 18. P=300 S=800 19. P=300 S=900 20. P=300 S=1000 21. P=300 S=1100

The overall layout of this experiment consisted of 7 cubes measuring 10mm x 10mm x 10mm, 4 rectangles formed from rectangular prisms measuring 1mm x 10mm x 10mm, 3mm x 10mm x 10mm, 5mm x 10mm x 10mm, and 6mm x 10mm x 10mm, a half circle with a 6mm diameter and a zig-zagged pattern measuring 1mm in width with each horizontal and vertical section measuring 3mm on Autodesk Fusion 360. The completed .STL file were oriented as shown in Figure 3.5 (A) and placed at the zero-height position on the Magics build plate. Hatch spacing was set to 10 μ m with a 10mm stripe width and all samples were given a 175W laser power and 125mm/s laser scanning speed. The completed ILT file was transferred to the AconityONE and translated to match Figure 3.5 (A). Defocus was manually changed through the AconityONE interface system to match settings given in Figure 3.5 (B).

3.6.4 GRADE 2 TITANIUM SUBSTRATE NITRIDING SANDWICHING EXPERIMENT

Parameters developed from previous experiments were utilized to nitride the surface of a wrought Grade 2 titanium substrate and melt a layer of Grade 23 Ti-6Al-4V on top of the nitride. Grade 2 substrates were sectioned from the stock material using the Brilliant 220 precision saw into smaller substrates measuring 40mm x 40mm x 13mm. A pocket was milled into the sectioned substrate's top face with the use of a HAAS Supermini2 from HAAS Automation (Oxnard CA, USA). The pocket was centered on the top face of the substrate measuring 30mm x 30mm x 0.050mm.

The nitriding process was performed following the setup described in section 3.2 Laser nitriding. Substrate mounting consisted of 4 identical Grade 2 substrates adhered to the build plate as seen in Figure 3.6 (A). Nitriding was performed on the bottom half of the milled pocket to allow for the view of the bonding interface between the powder layer with both nitrided substrate and non-nitrided substrate to be seen on the same cross-section.

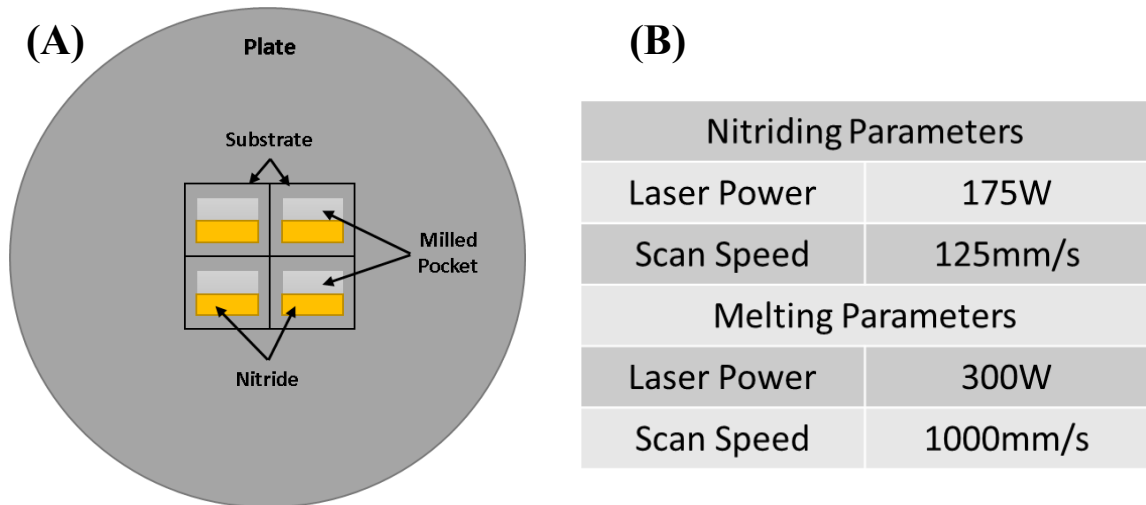


Figure 3.6 A) The orientation and position of substrates used during the substrate nitriding sandwich experiment. B) Lists the parameters for both the nitriding process as well as the melting of Ti-6Al-4V powder layer.

All substrates were nitrided using identical laser parameters as can be seen on Figure 3.6 (B). CAD files used for the nitriding stage were designed on Fusion360 with the use of rectangular prisms measuring 32mm x 16mm x 16mm. Parameters input into Magics utilized a 10 μ m hatch spacing, 10mm stripe width, with a laser power of 175W and 125mm/s scan speed.

After samples were nitrided, they were removed from the build platform to be photographed and examined to ensure the substrates had nitrided. After initial analysis, samples were placed in a small aluminum container to hold excess powder during the powder melting stage and mounted back onto the build platform in sets of two, samples 1 & 4 and samples 2 & 3. The milled pocket in the substrate was manually filled with Grade 23 Ti-6Al-4V powder. A hand held rake was used to distribute the powder in the milled pocket and provide a flat, even layer. CAD files for the melting were designed utilizing Fusion 360 in the shape of rectangular prisms measuring 32mm x 32mm x 16mm before being assigned laser parameters in Magics. The powder layer was then melted in two different environments. Samples 1 & 4 were melted after purging in

an argon environment and samples 2 & 3 were melted after purging in nitrogen. The fabrication laser parameters used for all powder melted utilizes a laser power level of 300W and a scanning speed of 1000mm/s.

These samples were all sectioned, mounted, and polished according to the process described in section 3.4. Finished samples were examined at the microstructure level following the section 3.5. With hardness measurements, data was collected using three consecutive indentations in a vertical orientation throughout the width of the sample's cross-section. Micro-indentations were made in close proximity for all three materials so they could be viewed simultaneously. The bottom indentation was made on the wrought Grade 2 titanium substrate, the second directly above it on the nitrided region of the substrate, and the last directly above the first two indentations on the Grade 23 Ti-6Al-4V melted layer. The measurements were designed to test for change in hardness values across the substrate.

3.6.5 GRADE 5 Ti-6Al-4V PULSED LASER EXPERIMENT

The pulsed laser experiments were designed to develop laser nitriding parameters to compare to the CW laser parameters. For this experiment, the Grade 5 substrate was cut from stock, and measured 150mm x 70mm x 30mm utilizing the HB280 Vertical band saw. Nitriding setup follows that of section 3.2 laser nitriding with the sectioned substrate being mounted on the build platform. Laser nitriding parameters utilized two sets or pulsed parameters. Nitriding orientation made use of 4 rows of squares that can be seen on Figure 3.7 (A). The top two rows each had a different set of laser parameters with a decreasing hatch spacing. The two bottom rows maintained a constant hatch spacing of 0.825mm, only varying the pulse width of the laser.

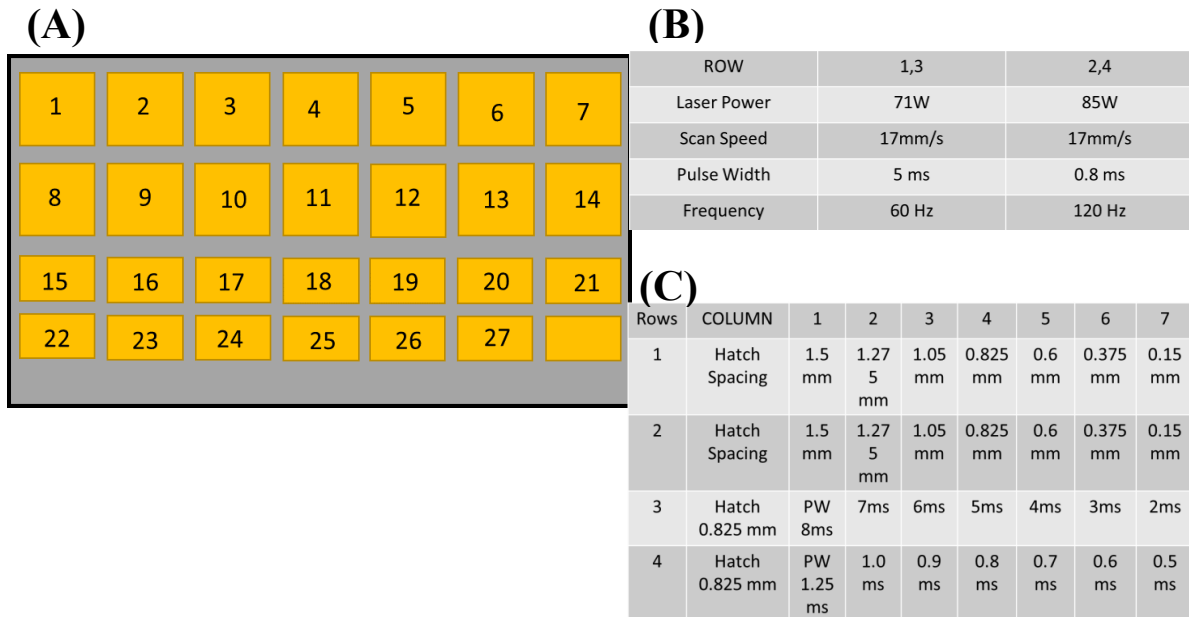


Figure 3.7 A) Displays the layout of nitrided cubes for the pulsed Ti-6Al-4V experiment. B) Details the 2 laser parameter sets used for the experiment. C) Lists the hatch spacing for each row as well as any changes made per sample.

Pulsed laser parameters had to be changed in the AconityONE interface however all changes in hatch spacing had to be done prior in slicing software. Initial CAD files were created using Fusion360 with a 10mm x 10mm x 10mm cube for the top two rows, and a smaller rectangle measuring 10mm x 7.5mm x 10mm for the bottom two rows displayed in Figure 3.7 (A). The smaller box was saved with a hatch spacing of 0.825mm, while the cubes were saved as 7 different files each with a hatch spacing corresponding to those show in Figure 3.7 (C). Files were then uploaded to the AconityONE system and arranged as shown in Figure 3.7 (A). Laser parameters were manually changed to pulsed configuration and modified to match laser parameters values shown in Figure 3.7 (B). and pulse width values for rows 3-4 shown in Figure 3.7 (C).

3.6.6 INITIAL GRADE 23 Ti-6Al-4V LPBF SURFACE NITRIDING

The first fabricated substrates utilizing the AconityONE system followed the setup procedure described in Section 3.1. A small build plate measuring 100mm in diameter was used to fabricate Ti-6Al-4V cubes that were subsequently used as substrates for nitriding. The build plate was centered on the build platform shown by the smaller circle indicated in Figure 3.8 (A). This was the first nitriding experiment conducted on a LPBF fabricated substrate. Parameters were selected using two CW laser parameters and two MW laser parameters from previous Grade 5 titanium nitriding that can be seen in Figure 3.8 (B). MW laser parameters were used on 12 cubes each with varying defocus values ranging from -10mm - +10mm. The CW laser parameters were performed on 2 cubes with a +/- 10mm defocus.

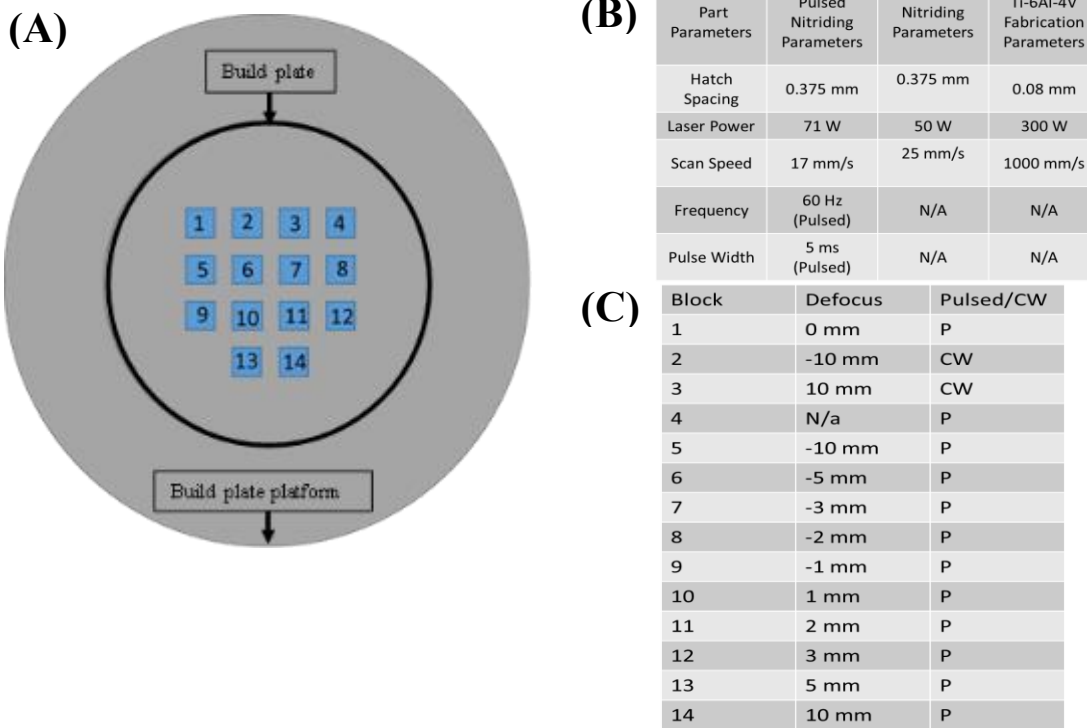


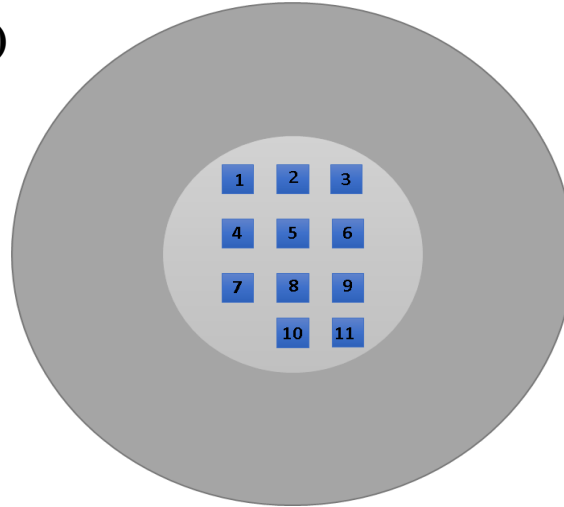
Figure 3.8 A) Demonstrates the locations of all cubes during the fabrication and nitriding process. B) Lists all parameters sets utilized for fabrication as well as base nitriding parameters. C) Lists the defocus values for each individual cube.

All part files designed for fabrication and nitriding were produced in Fusion 360 before being assigned parameters in Magics. The cubes used for fabrication were designed measuring 10mm x 10mm x 10mm. Squares that served as the base for the top nitride layer were designed to measure 7.5mm x 7.5mm to avoid nitriding close to the sample edges and avoid nitriding on powder. All base cubes were fabricated under the same building parameters listed in Figure 3.8 (B). Magics was utilized to slice model files and assign base parameters. Build files were assigned a 0.08 hatch spacing, 300W laser power, 1000mm/s scanning speed, layer height of 50µm. Two files were created for nitriding, one for the MW laser parameters and one for the CW parameters shown in Figure 3.8 (B). The AconityONE interface was used to arrange all cubes to match the image seen in Figure 3.8 (A), with nitriding files placed within the build files. Defocus values for individual cubes to values given by Figure 3.8 (C). were manually changed. Part fabrication was done for 100 layers to give a sample height of 5mm. At the end of fabrication, the chamber was purged with nitrogen according to the steps described in Section 3.2 Using this methodology, nitriding was conducted for a single layer on the top surface of the fabricated cubes.

3.6.7 FIRST Ti-6Al-4V/TiN SANDWICH BUILD

An experiment was designed to determine the effects and process to produce a multi-layer “sandwich” consisting of two nitride layers separated by ~6mm of LPBF deposited Ti-6Al-4V. The process combined the methodologies described in Section 3.1 and the Section 3.2 multiple times. The first sandwich experiment fabricated a small section of the sample measuring ~5mm, nitrided the surface, and repeated the process adding two more sections of fabricated Ti-6Al-4V with a nitrided layer in between. A total of 11 cubes were fabricated with a base sample set with no nitriding consisting of 3 cubes, two MW laser parameters each of 3 cubes, and 2 cubes with the use of CW laser parameters.

(A)



(B)

Part Parameter	Pulsed Nitriding Parameters		Continuous Nitriding Parameters	Ti-6Al-4V Fabrication Parameters
Laser Power	71W	85W	50w	300W
Scanning Speed	17mm/s	17mm/s	25mm/s	1000mm/s
Frequency	60Hz	120Hz	N/a	N/a
Pulse Width	5ms	0.8ms	N/a	N/a
Hatch Spacing	0.375mm	0.375mm	0.375	0.1mm
Defocus	0mm	0mm	+/- 10mm	0mm
Cubes	1,4,7	3,6,9	10,11	All

Figure 3.9 A) Demonstrates the locations of all cubes during the fabrication and nitriding process. B) Lists all parameters sets utilized for fabrication as well as base nitriding parameters.

Cubes 2, 5, and 8 were not nitrided during the process to act as a control group for the samples. These base samples served to detect any problems that may have occurred due to the time span between fabrication steps as well as any unintentional absorption of nitrogen into the substrate. Cubes were fabricated in argon until reaching a height of 5mm, then followed by a purge in nitrogen to form the first nitride layer. Next, the system was re-purged with argon to resume the standard Ti-6Al-4V building process until an additional 3mm of material were deposited. This was followed by a second purge in nitrogen to form the second nitride layer, before undergoing the last argon purge and a final fabrication of the top 2mm of Ti-6Al4V. The part files used during the initial powder build experiment were re-used from the previous experiment as all the samples and nitriding areas were to stay the same size. However, processing parameters for each cube were

changed in Magics. The base cubes used for the fabrication stages utilized the fabrication parameters presented in Figure 3.9 (B), while 3 nitriding files were produced; one for each of the three nitriding parameters sets also described in Figure 3.9 (B). Prepared files were arranged to meet the locations shown in Figure 3.9 (A). For this experiment the defocus value for cubes 10 and 11 was manually changed before processing.

3.6.8 SEQUENTIAL Ti-6Al-4V/TiN SANDWICH BUILDS

Sandwich builds were conducted a total of three times all following the steps of the first sandwich experiment, described in the previous section. The second setup was fabricated identically with the goal of studying the cracking within samples and determine possible causes for the cracking. The third sandwich experiment followed the same setup as its predecessors; however, a 67° angle rotation was added to laser scanning parameters. This variable had been preset at 180° by the slicing software as a standard parameter on initial builds and was changed to 67° to influence the laser scanning direction. This strategy has been used in the regular LPBF processing to lower thermal stresses.

3.6.9 Ti-6Al-4V/TiN SURFACE NITRIDING PARAMETER REFINEMENT

Nitride quality and threshold conditions were examined to narrow down changes produced by slight modifications within similar laser exposure parameters. The parameters in this experiment were designed to test the effects of scanning speed, input power, and beam overlap during the nitriding process. Two stages of the experiment were observed; Sample fabrication following the steps outlined in Section 3.1, followed by surface nitriding whose steps were outlined in Section 3.2.

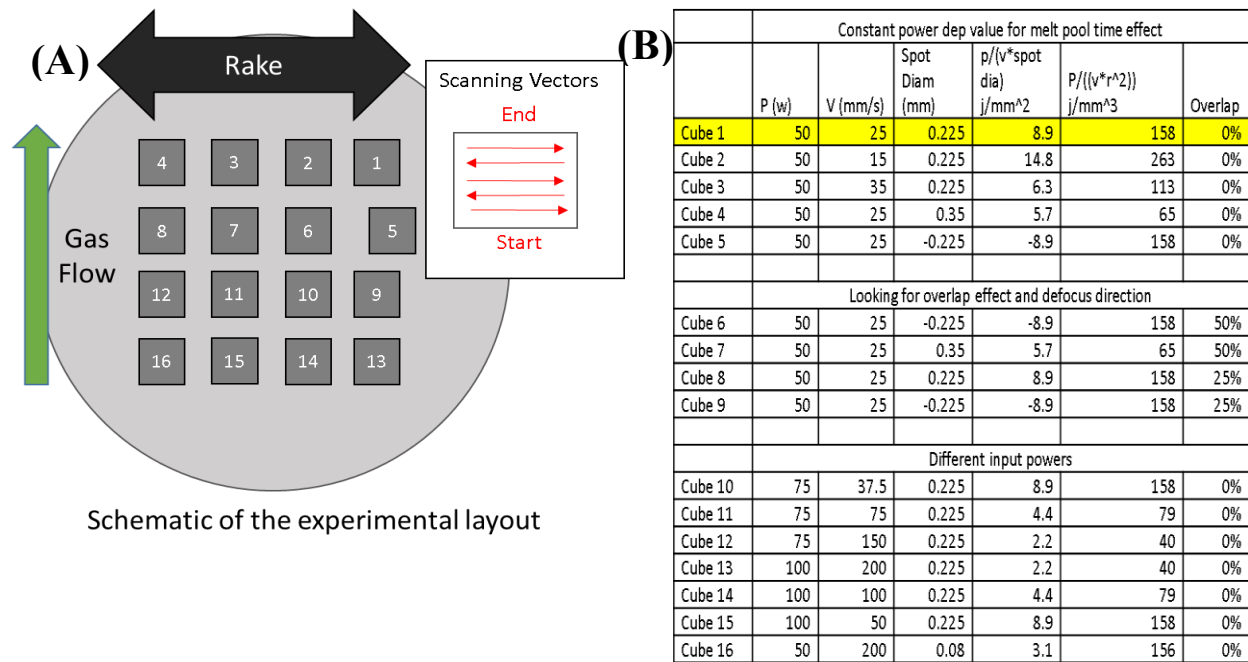


Figure 3.10 A) Demonstrates the locations of all cubes during the fabrication and nitriding process. B) Lists all parameters sets utilized during fabrication and nitriding with all variables that were modified.

A larger Ti-6Al-4V build plate measuring 150mm in diameter was used onto which samples were fabricated. Fabrication laser parameters were modified to better improve build microstructure and reduce internal flaws by increasing laser power to 330W while maintaining laser scanning speed at 1000mm/s. Samples were fabricated to have a height of 6mm before being nitrided in the orientation depicted in Figure 3.10 (A). A 67° rotation angle was used for the scanning direction to reduce thermal stresses and cracking in the samples. Fabrication followed procedures from Section 3.1, until the 10mm x 10mm x 6mm samples were complete. The surface nitriding followed procedures outlines in Section 3.2 utilizing the laser parameters seen in Figure 3.10 (B). These parameters were utilized to create each individual cube in Magics modeled from a Fusion360 part file measuring 10mm x 10mm x 6mm.

CHAPTER 4: RESULTS

4.1 PRELIMINARY GRADE 2 TITANIUM SUBSTRATE NITRIDING

Preliminary nitriding results on a wrought Grade 2 titanium substrate, depicted in Figure 4.1 (A), demonstrated a correlation between the scanning speed at which nitriding was performed and the uniformity of the surface nitride layer. Selectively nitrided sections with slower scanning speeds, as listed in Table 4.1 (B), demonstrated a more uniform nitride layer producing a more consistent golden color associated with TiN on the left side of the substrate as opposed to the right where minimal nitriding occurred with faster laser scanning speeds, the fastest of which scanned at 350mm/s. Excessive energy produced from slow scanning speed of 50mm/s during the nitriding process caused a blackening effect which can be seen on the surfaces of cubes 1, 8, and 15. Higher nitrogen content, which can be indicated by a golden color, while maintaining a smooth and consistent surface finish are the desired characteristics sought after when initially looking at surface nitriding. Cubes 2, 3, 9, and 10, demonstrated such properties and were nitrided with scanning speeds of 100mm/s and 150mm/s.

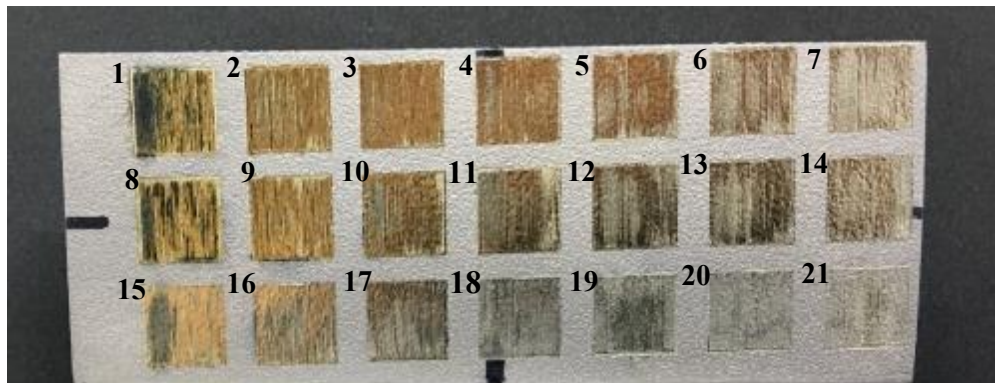


Figure 4.1 Resulting nitriding layer produced utilizing initial laser nitriding parameters by changing laser power and scanning speed

Table 4.1 Corresponding laser parameters for each sample in Figure 4.1

Cube	Laser Power	Scan Speed		Cube	Laser Power	Scan Speed
1	175	50		12	200	250
2	175	100		13	200	300
3	175	150		14	200	350
4	175	200		15	300	50
5	175	250		16	300	100
6	175	300		17	300	150
7	175	350		18	300	200
8	200	50		19	300	250
9	200	100		20	300	300
10	200	150		21	300	350
11	200	200				

4.2 PRELIMINARY GRADE 5 SUBSTRATE NITRIDING

Preliminary nitriding was performed in the Grade 5 Ti-6Al-4V utilizing the same parameters as those used for preliminary nitriding on a Grade 2 titanium substrate listed in Table 4.2. The nitrided substrate can be seen in Figure 4.2 (A). The nitriding parameters did not produce a consistent golden color on the Grade 5 substrates when compared to the Grade 2 substrates. This golden color is one of the main indicators that can identify nitriding. Rough patches were shown in all cubes, such as cube 6 in Figure 4.2 (A) where a large dark rough spot can be seen demonstrating further discoloration than the rest of the sample. Despite demonstrating less nitriding overall compared to the Grade 2 substrate, increased laser scanning speed did still show less golden color throughout the nitrided regions than those performed under slower scanning speeds.

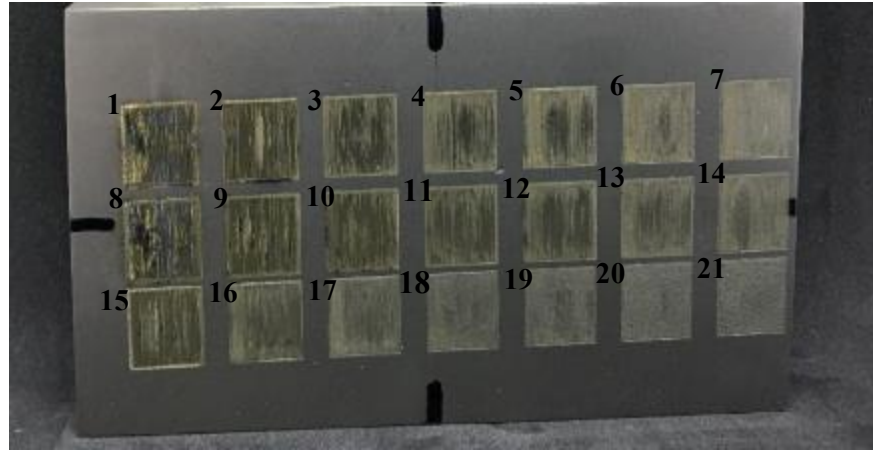


Figure 4.2 A) Resulting nitriding layer produced utilizing laser nitriding parameters by changing laser power and scanning speed.

Table 4.2 Corresponding laser parameters for samples in Figure 4.2

Cube	Laser Power	Scan Speed		Cube	Laser Power	Scan Speed
1	175	50		12	200	250
2	175	100		13	200	300
3	175	150		14	200	350
4	175	200		15	300	50
5	175	250		16	300	100
6	175	300		17	300	150
7	175	350		18	300	200
8	200	50		19	300	250
9	200	100		20	300	300
10	200	150		21	300	350
11	200	200				

4.3 SECOND GRADE 5 TITANIUM SUBSTRATE NITRIDING-DEFOCUS TESTING

Lack of nitriding on the wrought Grade 5 Ti-6Al-4V substrate showed that the process had insufficient power levels for nitriding. Scans caused by a change in beam defocus showed

promising nitriding opportunities as the larger beam diameter caused overlap between laser beam scans. The nitriding layers showed higher consistency as the samples proved to have fewer rough patches throughout the nitrided region, as well as less discolored areas. Despite the increase in layer consistency, the gold color produced by the nitriding process is not present. A contributing factor to this may be lack of nitrogen diffusion due to lower power caused by the defocus value. The defocus is responsible for increasing the area on which the laser beam energy is interacting with the substrate.

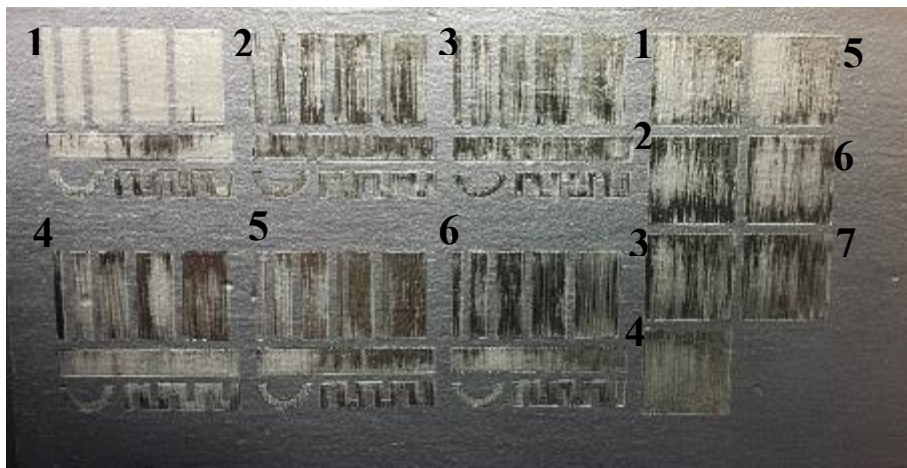


Figure 4.3 Resulting nitriding layer produced utilizing laser nitriding parameters by changing laser power, defocus, and scanning speed.

Table 4.3 Corresponding laser parameter settings for Figure 4.3

Laser Power	175W
Scan Speed	125mm/s
Part	Defocus
1	13.5
2	14.5
3	15.5
4	16.5
5	17.5
6	18.5
7	19.5

4.4 GRADE 2 TITANIUM SUBSTRATE NITRIDING SANDWICHING EXPERIMENT

4.4.1 NITRIDING AND POWDER FUSION RESULTS

Successful nitriding results produced from the preliminary nitriding parameters used on wrought Grade 2 Ti substrates were carried over to the initial sandwich experiment. The use of a defocus variable was used in an attempt to increase layer surface consistency with the use of overlap of laser beam passes. Misalignment of the laser beam caused for a shift in the location of the nitriding pattern in sample 1 shown as the top left samples in Figure 4.4 (A).

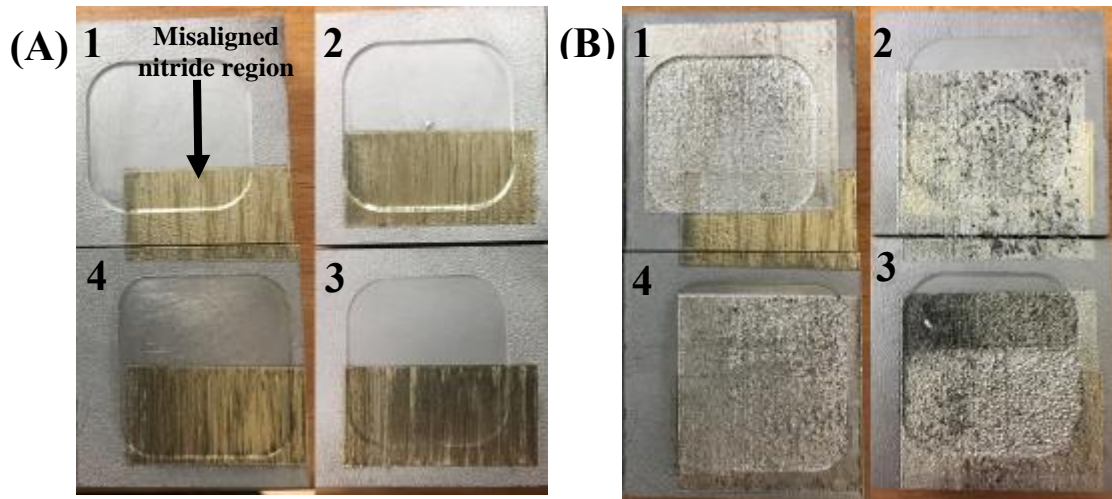


Figure 4.4 A) Depicts the samples post surface nitriding. B) Depicts samples after additional powder fusion has been performed on top of the nitrided surface.

Uniform nitriding was observed in all samples with minimal spots of discoloration in Figure 4.4 (A). After nitriding, powder was added to the pockets of the samples and were subsequently melted two samples at a time. Sample 3 in Figure 4.4 (B), demonstrated a burning effect on the top section of the milled pocket. This larger burnt section as well as small burnt sections located throughout sample 2 are thought to have been caused by residual nitrogen in the chamber that was not purged out from the nitriding process. For this experiment, sample 1 demonstrated the most uniform Ti-6Al-4V powder layer of all samples followed by sample 4. Due to the experimental setup, powder had to be applied to the milled section manually. Raking to distribute powder was also performed manually and could have caused an uneven layer. Possible deviations in the milled pocket from the milling process may have also contributed to the uneven powder layer. Manual raking was performed to spread powder and fill the milled pocket, however perfectly even distribution of the Ti-6Al-4V powder was not possible due to human error when raking.

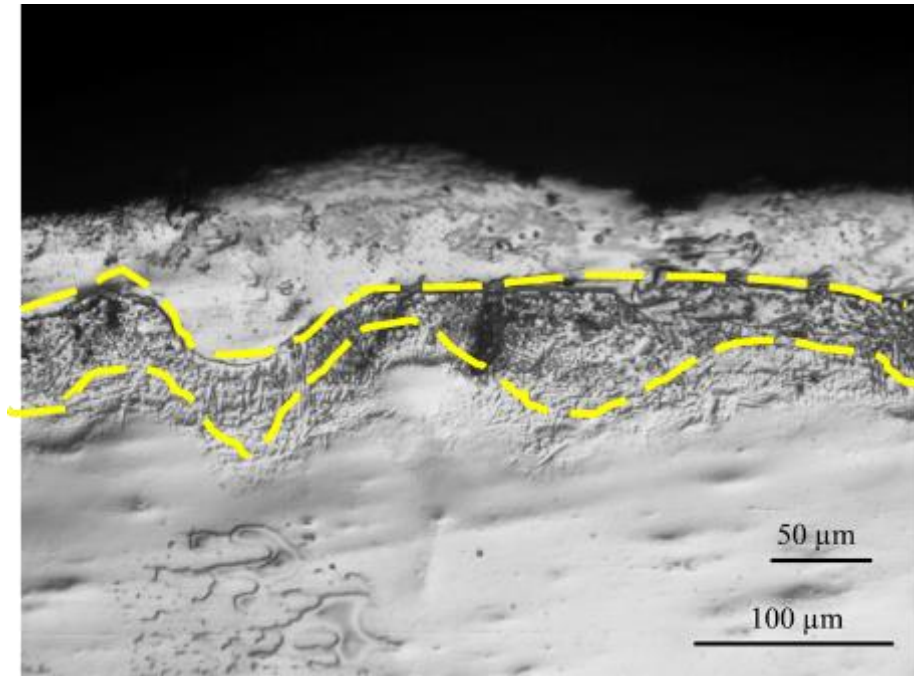


Figure 4.5 A zoomed in image at 20x magnification on an optical microscope with an added line to help separate the nitrided zone from the unaffected base substrate and the fused Ti-6Al-4V powder layer.

A dashed line in the micrograph in Figure 4.5 is used to show the approximate boundary line separating the different regions of the cross-sectioned samples. The nitride layers observed reached a depth ranging from $\sim 50\mu\text{m}$ - $75\mu\text{m}$ at the thickest regions. Upon more detailed examination of the nitrided area, dendrites are easily visible throughout. The dendrites, as can be seen in Figure 4.6 and 4.7, are confirmation of the successful results of selective nitriding (A Schultz, 2009). These dendrites structures revealed as white in the magnified microstructure can be seen in Figures 4.6 and 4.7, and are caused by the diffusion of the nitrogen and the formation of TiN.

More even distribution of TiN dendrites can be seen throughout the microstructure images presented in Figure 4.6 (B), (C), and (D). Figure 4.6 (A) however shows more densely packed regions that may be fused or interconnected dendrites. These areas with more densely packed

dendrites were found to have increased hardness than other surrounding areas. Additional microstructure images seen in Figure 4.7, show dendrite distributions as well as an overall microstructure view with the interactions between the Grade 2 Ti layer, TiN, and melted Ti-6Al-4V powder layer on top.

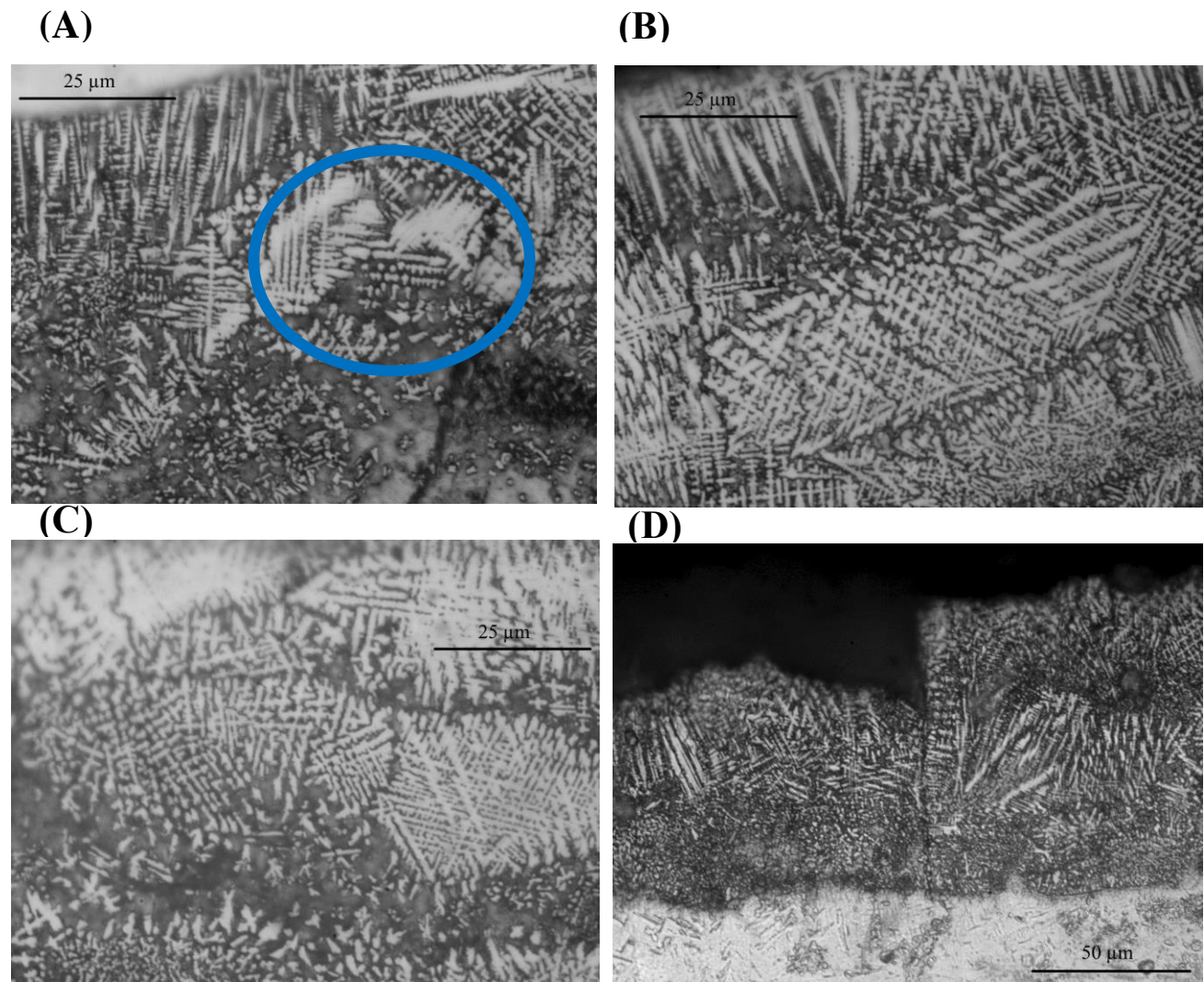


Figure 4.6 Demonstrates different sections of the dendrites within the TiN microstructure. A) Contains areas of higher dendrite concentration at 100X magnification circled in blue. B&C) show the more distributed view of dendrites within the microstructure at 100X magnification. D) A slightly zoomed out image at 50X magnification with an overall view of the TiN layer as well as the transition from the base Grade 2 substrate.

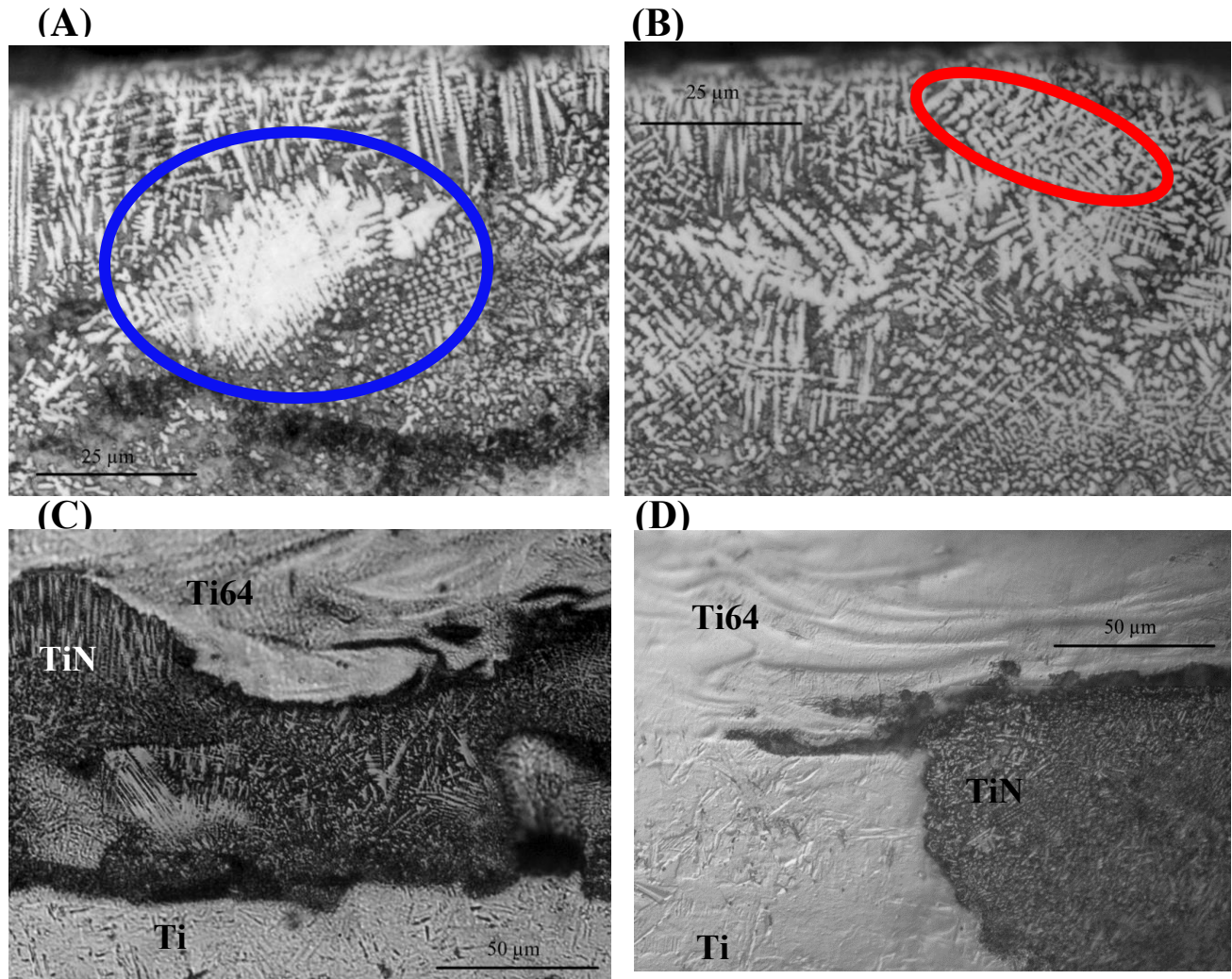


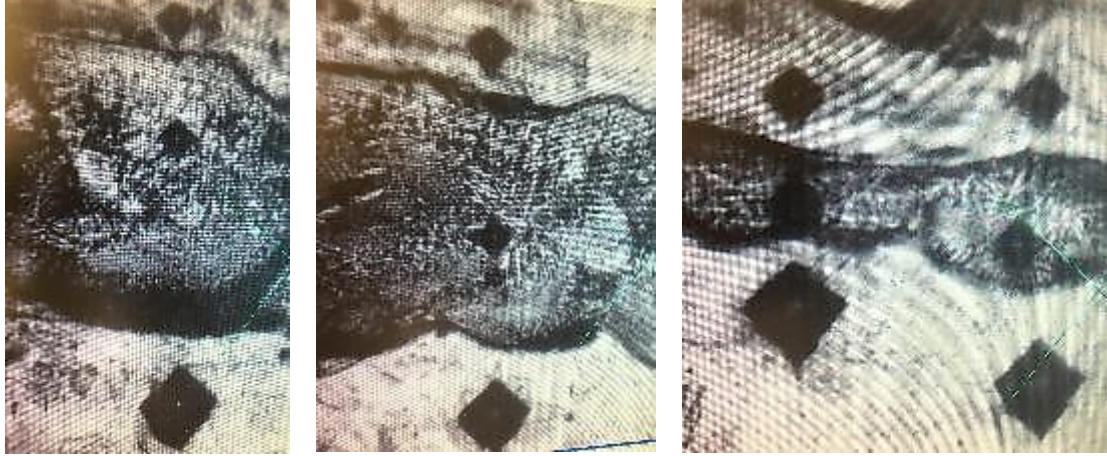
Figure 4.7 A) Highlights a large dendrite concentration $\sim 50\mu\text{m}$ in length as a point of increased material hardness among the surrounding nitrided area at 100X magnification. B) Demonstrates a more evenly distributed dendrite microstructure with larger individual dendrites at 100X magnification. C&D) Provide an overview of the interactions between the sample materials along the cross-section surface. The interaction in the middle of the nitride layer can be seen in (C), while the farthest edge of the nitride can be seen in (D).

4.4.2 HARDNESS TESTING

Hardness Testing was conducted on the sectioned samples in sets of 3 indentations. Each indentation was aligned along the vertical direction of the cross section depicted in the microstructure images on each of the sample materials. Sets of indentations were performed to

be able to correlate results between the materials and to detect regions that may be weaker than the rest of the layer. These indentations can be observed in Figure 4.8 (A) and a substantial increase in size of the micro-indentations between the base Ti substrate when compared to those performed on the TiN and Ti-6Al-4V sections of the substrate. The resulting Ti micro-hardness values seen in Figure 4.8 (B) are also shown to be of substantially lower than the TiN and Ti-6Al-4V region values averaging ~440-495 VHN. The indentations performed on the TiN show the smallest indentation size as well as the highest corresponding micro-hardness values of all measurements taken at ~1200-1800VHN. Micro-hardness measurements taken on the top layer of Ti-6Al-4V show unusually high hardness values between ~1000-1200VHN. These values may be attributed to higher than normal levels of residual nitrogen in the fabrication chamber during fabrication as well as only having a single Ti-6Al-4V layer where all nitrogen diffused during fabrication will have stayed in that surface layer.

(A)



(B)

Sample	1A				2A		
Material	Ti	Ti-6Al-4V	TiN		Ti	Ti-6Al-4V	TiN
Hardness	430	1060	1167		511	1117	1420
	416	1017	1292		507	1193	1338
	430	1117	1292		450	1322	1609
	444	1071	1338		526	1038	1262
	493	1038	1839		493	1180	1529
	424	1154	1814		473	1277	1789
Average Hardness	439.5	1076.167	1457		493.3333	1187.833	1491.167
SD	25.34923	46.49522	266.4845		25.35525	94.43413	175.624

Figure 4.8 A) Displays the micro-indentations performed on the substrates across three materials along a single axis. B) Displays the individual, and average hardness measurements taken from the micro-indentations on two separate samples; 1 and 2 from Figure 4.5.

4.5 GRADE 5 Ti-6Al-4V PULSED LASER EXPERIMENT

Pulsed laser parameters were utilized in an attempt to produce more apparent nitriding on wrought Grade 5 Ti-6Al-4V substrates. The MW laser parameters, shown in Table 4.9, utilized two different parameters sets each with varying hatch spacings or pulse widths. The resulting samples provided a substantial improvement as a clear golden color can be seen in the sample surfaces, as shown in Figure 4.9 (A), after the nitriding process. Varying line widths were produced within individual line scans of the nitrided regions. Of the samples produced, samples 2 and 9 shown as the far-left squares in Figure 4.9, produced very clear, consistent line widths. While

varying widths, such as those seen in samples 6 and 13 gave the appearance of dull patches. These dull patches were a result of changes in line widths that created thin gaps between scans where the titanium substrate can be seen. Areas with more consistent line widths produced a smoother golden surface. Samples 7 and 14 produced high levels overlap causing charring and making it near impossible to differentiate between individual line scans.

The width of each line scan was measured at 5 different points on 5 lines per square. The resulting data collected did not show any consistent pattern related to laser parameter or hatch spacing other than the samples with the largest hatch spacings that showed uniform size throughout. All other width measurements and deviation in width fluctuated back and forth and can be seen in Figure 4.10.

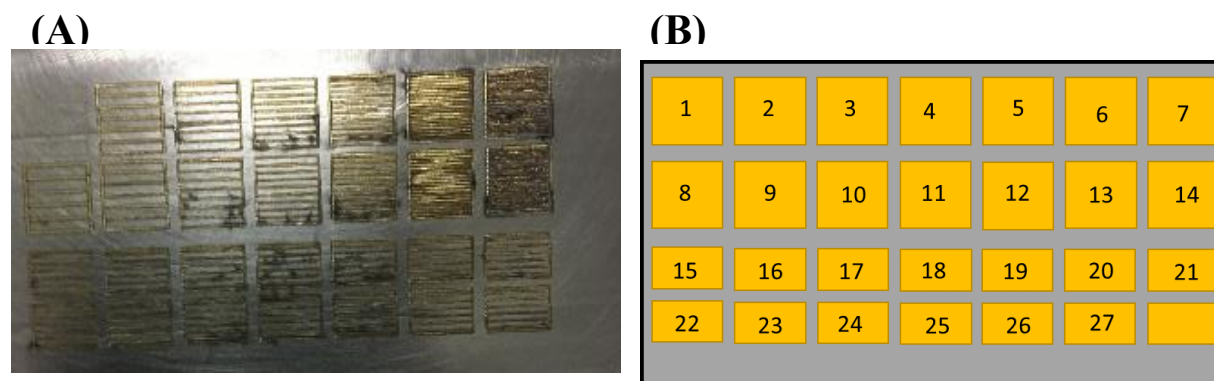


Figure 4.9 A) Displays the nitrided Grade 5 substrate after nitriding utilizing a pulsed laser configuration. B) Displays the corresponding sample setup used for the pulsed laser nitriding.

Table 4.5.1 Lists corresponding laser parameters for samples in Figure 4.9

ROW		1,3				2,4		
Laser Power		71W				85W		
Scan Speed		17mm/s				17mm/s		
Pulse Width		5 ms				0.8 ms		
Frequency		60 Hz				120 Hz		
Rows	COLUMN	1	2	3	4	5	6	7
1	Hatch Spacing	1.5 mm	1.27 5 mm	1.05 mm	0.825 mm	0.6 mm	0.375 mm	0.15 mm
2	Hatch Spacing	1.5 mm	1.27 5 mm	1.05 mm	0.825 mm	0.6 mm	0.375 mm	0.15 mm
3	Hatch 0.825 mm	PW 8ms	7ms	6ms	5ms	4ms	3ms	2ms
4	Hatch 0.825 mm	PW 1.25 ms	1.0 ms	0.9 ms	0.8 ms	0.7 ms	0.6 ms	0.5 ms



Figure 4.10 Plots the data collected from measuring the width of single pass laser scans on all samples based on laser parameter and standard deviation for each hatch spacing.

4.6 INITIAL GRADE 23 Ti-6AL-4V POWDER BUILD SURFACE NITRIDING

Initial surface nitriding on a LPBF fabricated substrate was used to test laser parameters to ensure consistent and effective formation of a single layer of nitride before sandwiching was attempted. Pulsed laser parameters from the wrought Grade 5 nitriding experiment were used with a modification in defocus to close minor gaps and improve nitriding finish. Two CW parameters, at 50W and 25mm/s with a positive and negative 10mm defocus, were included to compare the effects of CW to MW laser parameters as seen in Figure 4.11. The resulting nitrided samples showed a lack of nitrogen diffusion into all of the pulsed laser cubes due to the silver surface color while the continuous laser parameters produced a golden layer.

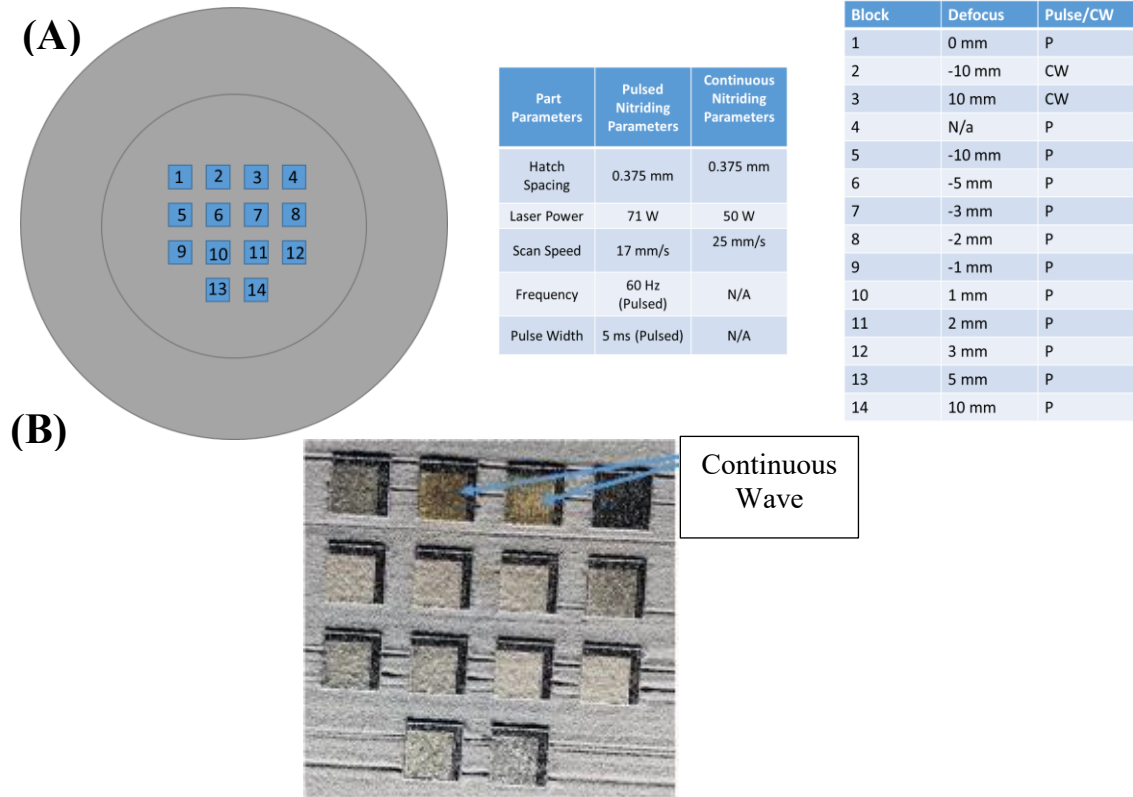


Figure 4.11 A) Shows the orientation for samples used during experiment setup. B) Displays the overall results post nitriding.

Cube 1 was nitrided utilizing a pulsed laser parameter set without the use of a defocus setting. The melt pool does not show a dendritic structure but still displays a melting zone deeper than any other parameter due to the 80 μm beam diameter having a more concentrated laser energy and is shown in Figure 4.12 (A). However, the short solidification time caused for limited nitrogen diffusion as minimal to no dendrite formation was observed in the microstructure of this MW laser parameter setting and is shown in Figure 4.12 (A). Similar to previous samples in this experiment, the heat affected zone can be seen around the melt pool in Figure 4.12 (B) with an average depth of 270 μm , the deepest of all heat affected zone boundaries. The nitride affected region shown in Figure 4.12 (C) shows deep penetration into the substrate similar to Figure 4.12 (A), but contains a different solidification geometry in the form of swirled patterns. The pattern gives a visual aid into how flow of the metal behaved during the nitriding process. At a depth of $\sim 70\mu\text{m}$, only a melt zone is observed with no dendrite formation. This may be due to increased depth where nitrogen was not able to diffuse to that depth during the regions melted state.

Cube 1			Spot Diameter (mm)	Frequency (Hz)	Pulse Width (ms)
	P (w)	V (mm/s)			
	71	17	0.08	60	5

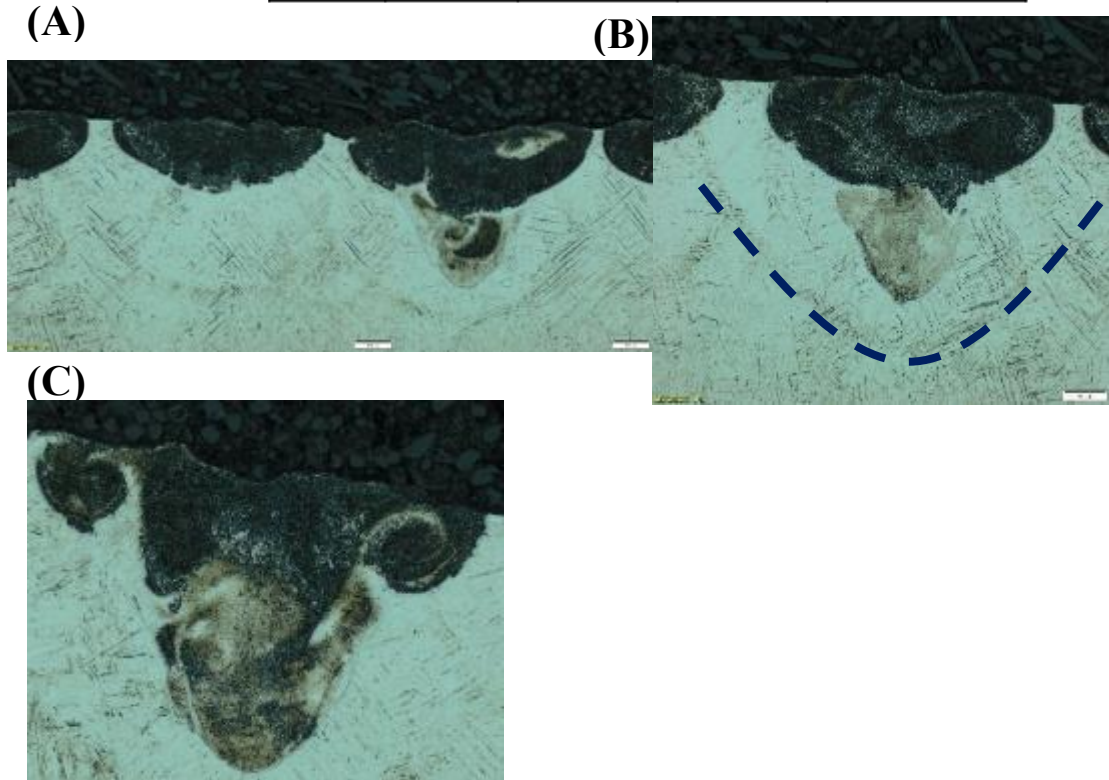


Figure 4.12 A) Depicts two laser scans. The difference in shape is due to the pulses not being parallel and only the edge of the let pool on the left being shown on the cross-section and not at its deepest penetration. B) Shows a more detailed view of a melt pool as well as the outline of the heat affected zone. C) Shows an enlarged view of the melt pool displaying the microstructure as well as some flow within the melt pool.

Cube 2, Figure 4.13, was examined to reveal a melt pool $\sim 85\mu\text{m}$. A thin nitride layer can be observed in Figure 4.13 (A) with evidence of a heat affected zone surrounding it shown as a phase change seen a semi-circular pattern. This heat affected zone is indicated by a dashed line and located directly below the nitrided region. This nitrided region can be seen in Figure 4.13 (B) under 20X magnification. Here a dendritic microstructure can be observed throughout the thin nitride layer once again confirming successful nitriding. The nitriding was also previously determined by the distinct golden color. The negative defocus values used for the laser parameters

creates a diverging laser beam. This reduces the energy directed into the substrate and can explain the lack of penetration into the substrate. The varying shapes of the melt pools in Figure 4.13 can be separated into two different categories. Melt pool geometries similar to that shown in Figure 4.13 (A), are thought to be a result from high melting temperatures and a large Marangoni number. Melt pool geometries similar to that seen in Figure 4.13 (B), are thought to have been caused by low thermal diffusivity preventing the thermal energy from penetrating further into the substrate and a high Prandtl number.

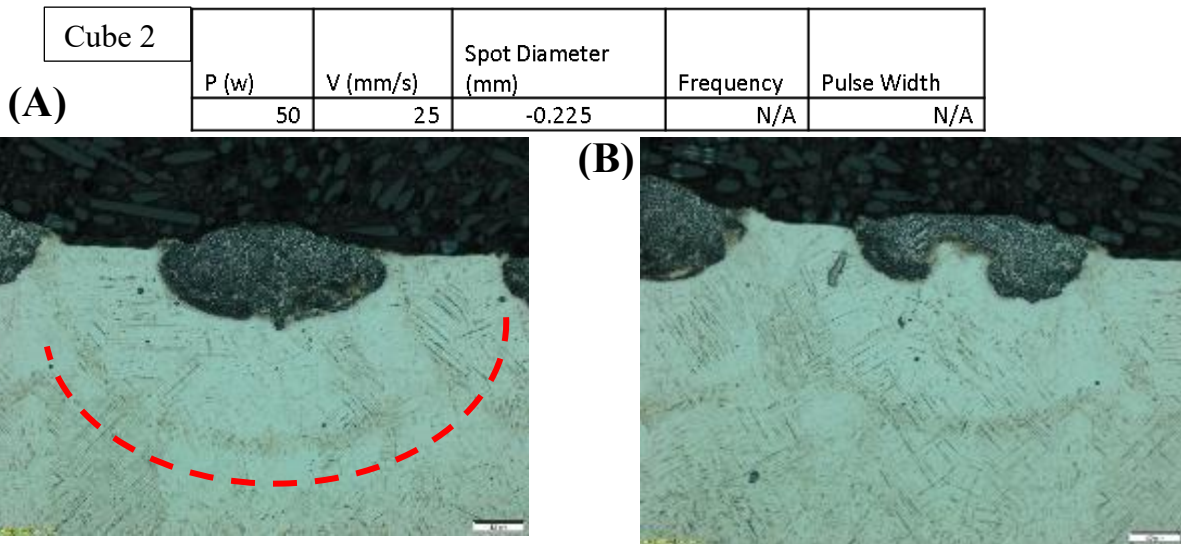


Figure 4.13 A) Displays the nitrided area at 10X magnification. The dotted red line lies on the border of the heat affected zone. B) Shows a different melt pool of the nitrided region at 10X magnification.

Cube 3 seen in Figure 4.14, followed the same laser parameters as those used for cube 2, with the exception of the defocus value. The modified defocus value was positive in this sample and gave the laser beam a converging profile. The effects of this can be seen as the nitrided region shows a shallower penetration averaging $\sim 52\mu\text{m}$ in depth. Two laser scans can be seen at 20X magnification next to each other in Figure 4.14 (A) with the heat affected zone shown as a dark semi-circular shape beneath each melt pool. These zones are located directly above two dashed

lines for easier visualization. Upon more thorough examination, two melt pool patterns can be seen in multiple laser passes.

Cube 3			Spot Diameter (mm)		
	P (w)	V (mm/s)		Frequency	Pulse Width
	50	25	0.225	N/A	N/A

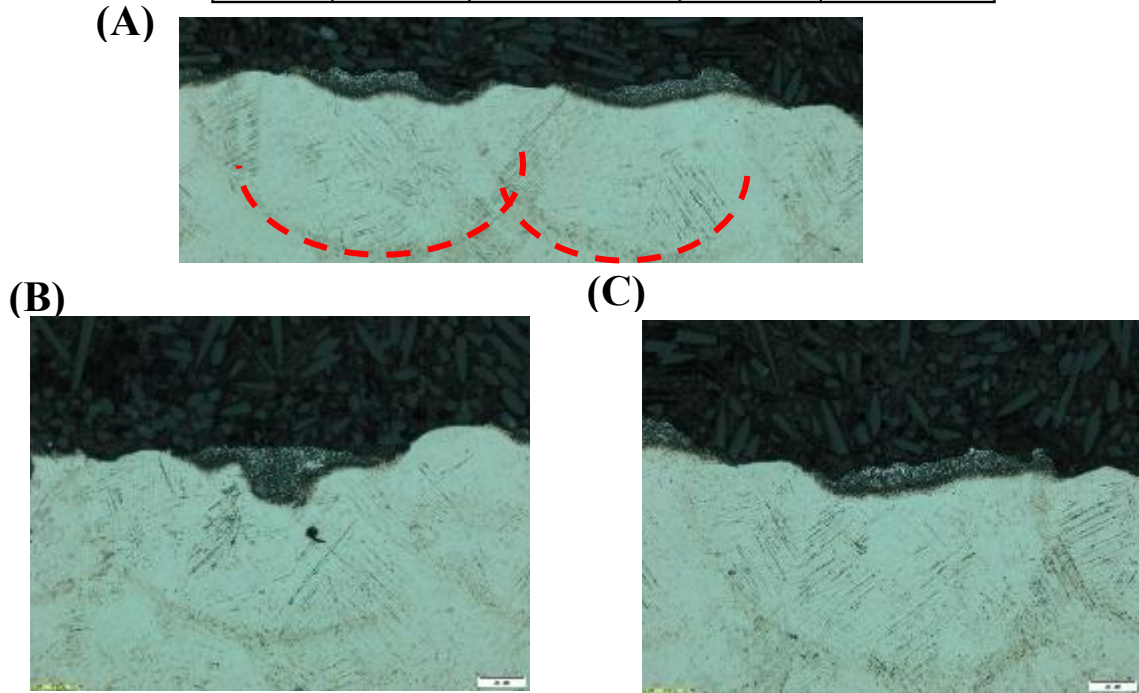


Figure 4.14 A) Displays the nitrided area at 20X magnification. The dotted red line lies on the border of the heat affected zone. B) Shows the nitrided region at 20X magnification where dendrites can be seen and is one of the two observed melt pool shapes. C) Displays the nitrided area at 20X magnification and depicts a different melt pool shape.

Cube 5 produced a more visible flow within the melt pool. At a magnification of 20X, Figure 4.15 (A), shows two melt pools with a depth of $\sim 65\mu\text{m}$ where a swirled pattern can be observed. These patterns are believed to follow the flow of the material while it was in its liquid state during the nitriding process. The melt pool located on the right side of the cross section, magnified in Figure 4.15 (B), has a very distinct swirl pattern indicating a vortex in the melt pool.

On the left side, dendrites can be seen while the right side does not have any dendrites and instead displays a swirled region depicting the vortex flow of the molten material during the nitrogen gas diffused into molten titanium. The cause of the swirled pattern is due to the vortices in the melt pool during solidification (A R Nassar, 2012). The pattern shows the mixture of titanium and nitrogen affected titanium. The displacement of the melted materials towards the edges of the melt pool can be partially explained through the Prandtl number theory referenced in chapter 2. This theory infers that when strong convection flow is present in the melt pool geometry, the thermal diffusivity is low and the Prandtl number is high. In this case the flow of the vortex currents within the melt pool flow towards the outside of the melt pool moving from hotter to cooler regions due to higher surface tension and a decrease in temperature. These hot liquids can be seen moving away from the center of the melt pool where energy is being introduced towards the edges causing the regions directly underneath to melt (A R Nassar, 2012). This sample was the only sample to exhibit a swirled melt pool however the majority of melt pools for this sample displayed melt pools similar to the melt pool located on the left in Figure 4.15 (A).

Cube 5		Spot Diameter (mm)	Frequency (Hz)	Pulse Width (ms)
P (w)	V (mm/s)			
71	17	-0.225	60	5

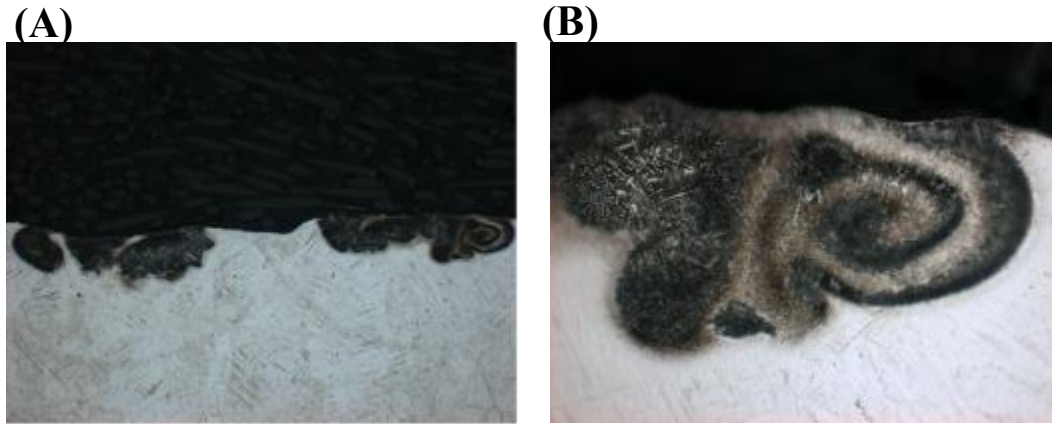


Figure 4.15 A) Overview of melt pools in the cross section. B) A magnified view of a swirled melt pool pattern demonstrating flow.

Cube 14 demonstrated signs of nitrogen content due to the dendrite formation seen in Figure 4.16. The melt pool geometry seen in Figure 4.16 (A) closely resemble those seen in Cube 2 and 5 where flow of the melted materials flows towards the outside of the melt pool. The melt pool geometry is quite similar to previous melt pools that exhibit behavior caused by having low thermal diffusivity and a high Prandtl number however, more dendrites can be seen throughout the melt pool. . Although slightly different in shape, both melt pools displayed in Figure 4.16 (A) and Figure 4.16 (B) share a similar melt pool geometry and have their concentration of dendrites located on the far sides of the melt pool with the center part having an absence of dendrites. Figure 4.14 (B) in particular showed less dendrites towards the center of the melt pool.

Cube 14			Spot Diameter (mm)	Frequency (Hz)	Pulse Width (ms)
	P (w)	V (mm/s)			
	71	17	0.225	60	5

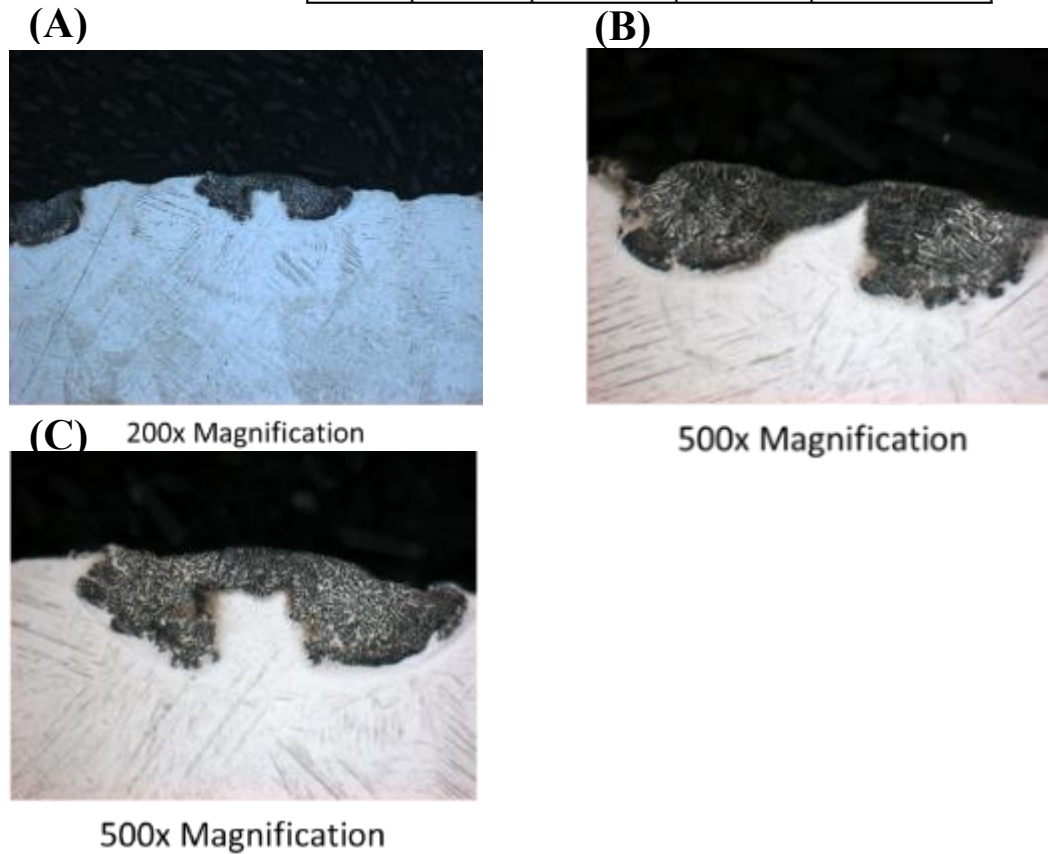


Figure 4.16 A) Overview of melt pools in the cross section.
 B) A magnified view of a swirled melt pool pattern demonstrating flow.

All melt pools were observed to compare the penetration of the melt pools between different defocus levels as well as the variation in melt pool geometry from within the same samples. The melt pools for -10mm, 0mm, and +10mm defocus values are shown in Figure 4.17 and includes CW and MW laser parameters. The resulting melt pools obtained show the MW laser parameter at zero defocus to have the deepest melt pool penetration at $\sim 175\mu\text{m}$ due to the energy being concentrated on a smaller beam spot. The geometry of the melt pool shown in the cross section is a two-dimensional representation of a three-dimensional melt pool. The region of

the melt pool that is viewed is dependent on the location at which the sample is sectioned. The CW and MW parameters at +/- 10mm defocus showed less penetration all <100µm. The samples showed less penetration into the sample at +10mm defocus averaging ~48µm and ~51µm for the MW and CW respectively as compared to -10mm defocus averaging ~65µm and ~86µm for the MW and CW respectively. Dendrites were more present in the samples nitrided with CW parameters samples when compared to those nitrided using MW parameters.

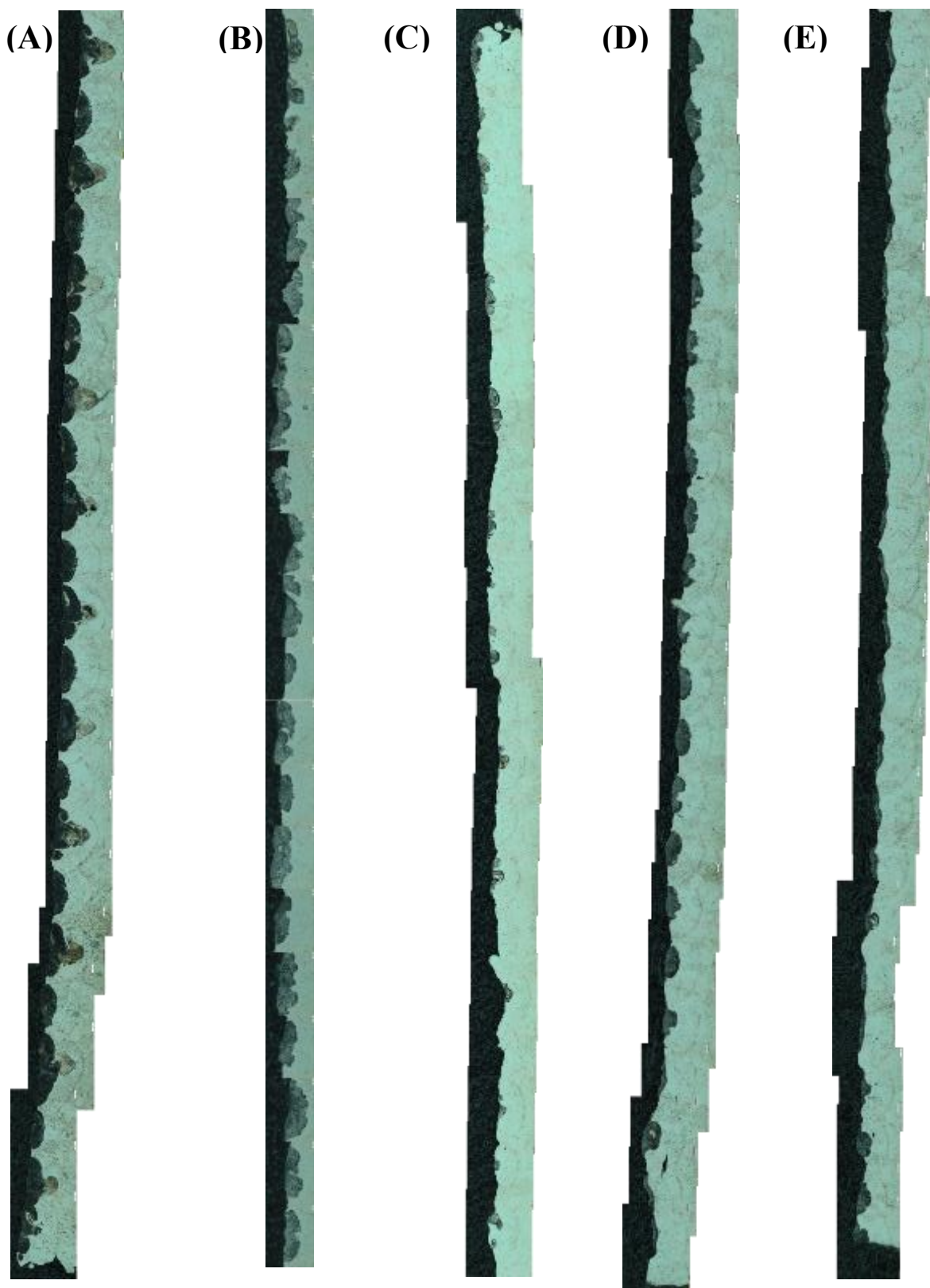


Figure 4.17 A) Pulsed laser parameters at 0mm defocus. B) Pulsed laser parameters at -10mm defocus. C) Pulsed laser parameters at +10mm defocus. D CW laser parameters at -10mm defocus. E) CW laser parameters at +10mm defocus.

The average melt pool depths were measured from all samples and shown graphically in Figure 4.18. A total of 44 data points were collected for each sample consisting of 22 melt pool measurements and 22 heat affected zone measurements. The graph demonstrates the correlation between defocus and average melt pool depth, with error bars showing the standard deviation calculated from all measurements taken. These values will include some variation between melt pools as it is measurements taken from the geometry on a two-dimensional plane of a three-dimensional melt pool. The deepest melt pools measured were from the MW laser parameter with 0 defocus at $\sim 175\mu\text{m}$ and a steadily decreases melt pool depth as defocus values are increased in both defocus directions. The CW laser melt pools produced melt pools deeper than their MW laser counterparts, however all laser parameters at $\pm 10\text{mm}$ defocus were the shallowest melt pools out of all samples.

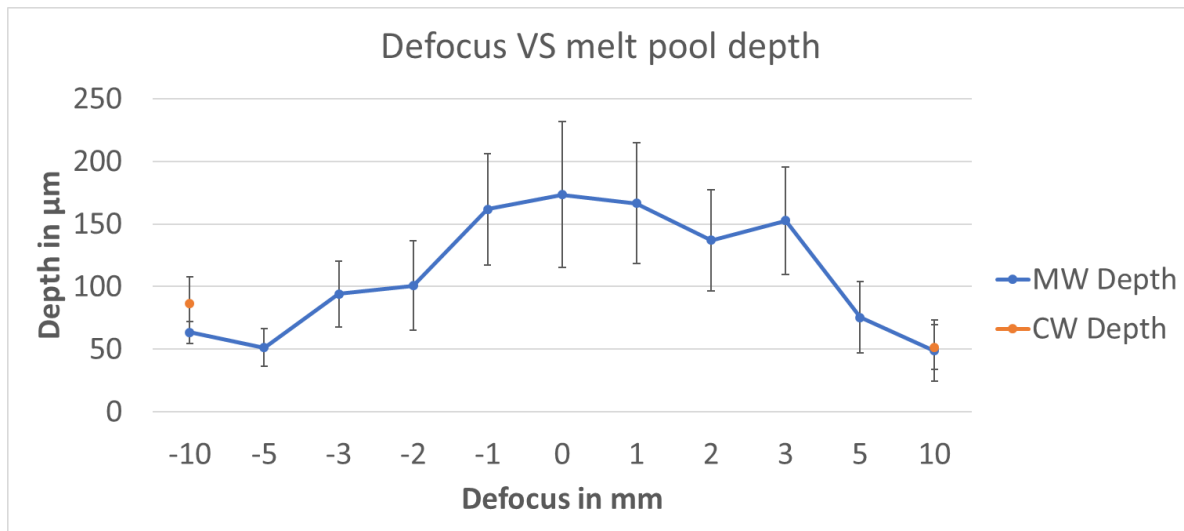


Figure 4.18 Plot comparing melt pool depth to defocus values with the standard deviation for each sample.

The average depth measured from the heat affected zones for each melt pool can be seen graphically in Figure 4.18 The average depth shows a correlation to the depth of the melt pools

as depth increases as the defocus value gets closer to 0mm. Depth of heat affected zones was shown to be ~100 μ m deeper for CW laser parameters than for MW laser parameters. Standard deviation was lower for the heat affected zones than those for the melt pool depth.

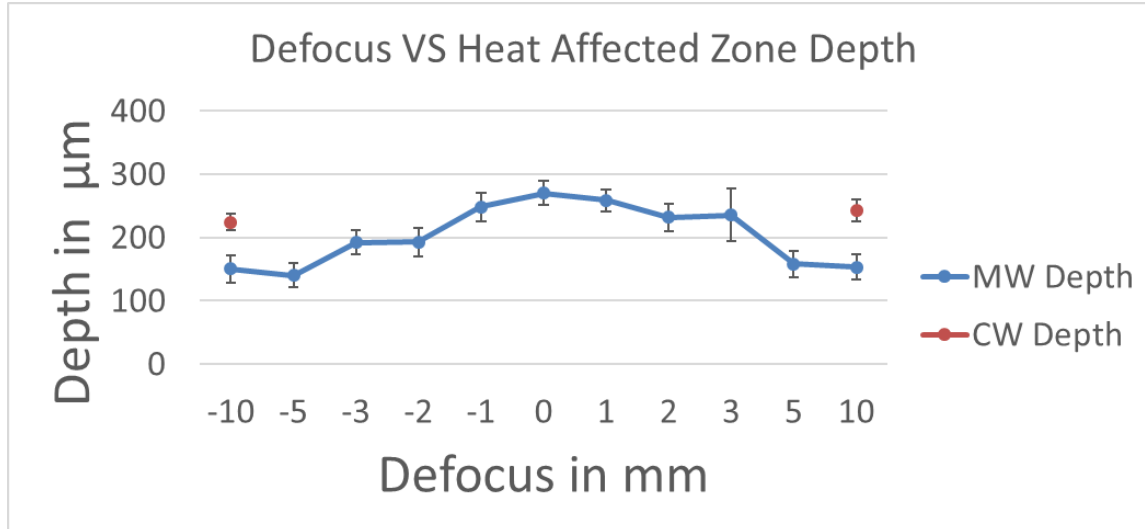


Figure 4.19 Plot comparing heat affected zone depth to defocus compared to the standard deviation.

4.7 SANDWICH EXPERIMENT 1

The initial sandwich build was the first experiment to attempt two layers of nitride within a build. Sample cubes were fabricated using CW laser parameters of 300W and 1000mm/s to melt Ti-6Al-4V layers. Two MW laser parameter sets, and one CW laser parameter set, shown in Table 4.20, were used to form the nitride layers within a nitrogen atmosphere. High stress levels during the cube fabrication process were caused by an over-rotation of the laser beam scanning angle of 180°, melting in the same directions causing internal thermal stresses to pile up and cause cracking in all samples produced. CW nitriding parameters were the only parameters observed to produce dendrites within the microstructure and were examined more in depth to view nitriding results as well as test for defects.

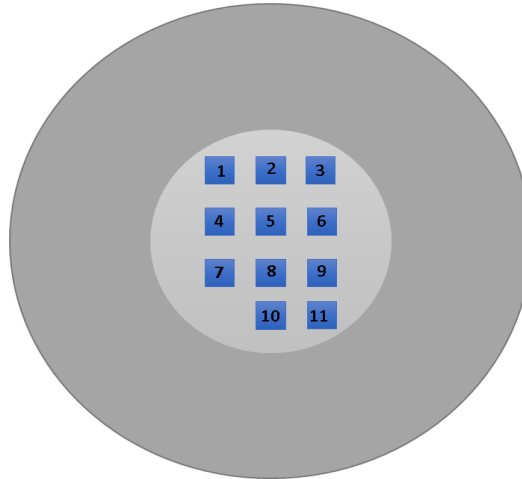


Figure 4.20 Depicts the orientation of samples arranged for the initial multi-layer nitride build with parameters run for each.

Table 4.7 Lists the laser parameters used in Figure 4.20

Part Parameter	Pulsed Nitriding Parameters		Continuous Nitriding Parameters	Ti-6Al-4V Fabrication Parameters
Laser Power	71W	85W	50w	300W
Scanning Speed	17mm/s	17mm/s	25mm/s	1000mm/s
Frequency	60Hz	120Hz	N/a	N/a
Pulse Width	5ms	0.8ms	N/a	N/a
Hatch Spacing	0.375mm	0.375mm	0.375	0.1mm
Defocus	0mm	0mm	+/- 10mm	0mm
Cubes	1,4,7	3,6,9	10,11	All

Cube 2 was a sandwich sample in which no nitriding was performed and only used fabrication parameters. This sample showed less external cracking compared to other samples. This sample was used as a base to compare the locations of cracking or other defects to their location along the height of the sample to see if they were initiated around nitrided regions. No defects were seen in this sample that were not seen in other samples and vice versa as all samples showed cracking throughout. The experimental goal was to fabricate sandwich structures and look at the effects of depositing Ti-6Al-4V on top of TiN and having a non-nitrided structure serves as a sample to check the normal formation of the cubes.

Cube 10 was a CW parameter sample which utilized a negative defocus value and successfully formed dendrites as can be seen in Figure 4.21. The individual laser scans produced a relatively uniform cross-section view with no major changes in shape from one scan to the next and can be seen in Figure 4.21 (A). Upon magnification of the image, interaction between laser scans can be observed due to some overlap as seen in Figure 4.21 (B). The CW laser parameters succeeded in nitriding the substrate showing evidence of dendrites within the microstructure, as shown in Figure 4.21 (C). The dendrites are small but are still present after additional Ti-6Al-4V layers are deposited.

Cube 10

Parameters:

50w
25mm/s
-10 defocus
Continuous wave
375 μ m hatch spacing

(A)



50x magnification

(B)



200x magnification

(C)



500x magnification

Figure 4.21 A) Shows a wide view of the nitride layer with multiple laser scans. B) Demonstrates a connecting behavior between melt pools. C) A magnified image for inspection of the microstructure in a melt pool.

Cube 11 utilized the continuous wave laser parameters and successfully produced dendrites within the microstructure. As can be seen in Figure 4.22, the crack was produced initiating from the nitride layer within the samples. However, not all cracks were centered around nitrified areas within the cube. The additional concentrated energy used during the nitriding process as well as differences in the coefficient of thermal expansion between the TiN and Ti-6Al-4V, may have contributed to the crack growth. The primary cause of the cracks was the scanning angle repeatedly scanning the same regions without rotation for the duration of the fabrication process as experiments performed utilizing a rotating scanning angle did not show

any visual external cracking while all experiments with a 180° scanning angle showed cracking internally and externally for all samples.

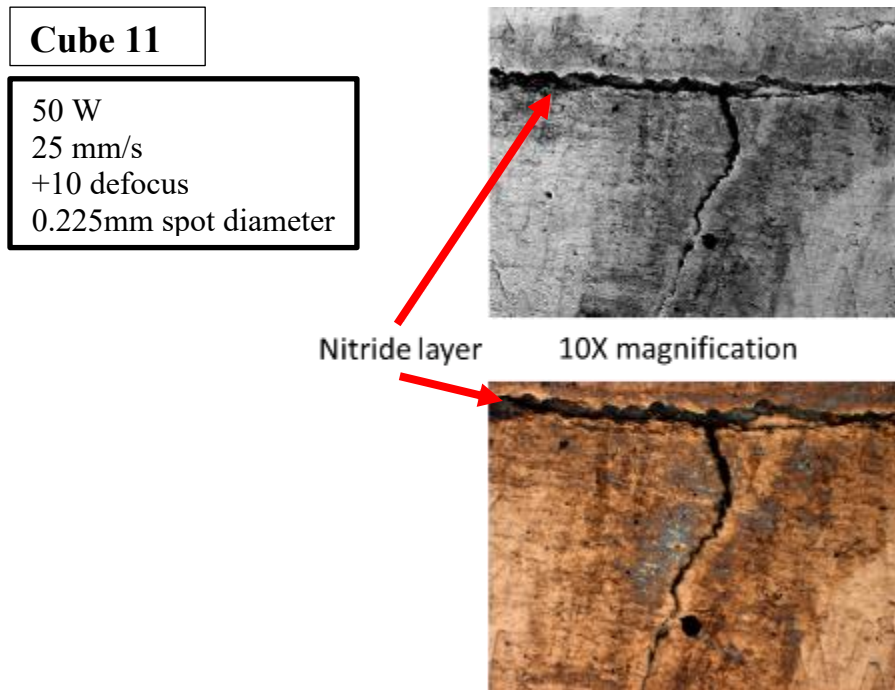


Figure 4.22 shows images taken from 2 microscopes at 10X magnification of a crack growth stemming from the nitride layer.

A hardness map was created by taking 13 microhardness measurements along the build direction across 5 columns spanning the horizontal length of samples 10 and 11 where dendrites were more prevalent. The Ti-6Al-4V substrate hardness ranged from ~450VHN to 550VHN, while the nitrided regions hardness ranged from ~600VHN to ~1300VHN. The relatively low hardness values of the nitrided regions as indicated in Figure 4.23 (A) are thought to have been caused by the TiN dendrites forming a composite with the Ti-6Al-4V and lowering the overall hardness of the region. The micro indenter is too large to take hardness measurements of individual dendrites within the TiN region so all values reflect the hardness of the entire melt pool region. Regions located directly above nitride layers showed normal hardness values expected for Ti-6Al-4V. The regions directly below nitrided layers show an increase in hardness

values, although only of ~50VHN above the surrounding Ti-6Al-4V layers. This could be explained due to diffusion of nitrogen into the substrate from the nitriding process creating nitrogen rich titanium or alpha prime phase TiN with slightly increasing hardness compared to the other regions of the substrate. The highest hardness value was measured in the dendritic region in Figure 4.23 (B). Other micro indentations made such as Figures 4.23 (C) and Figure 4.23 (D), showed an increase in hardness from the values of the base substrate. Overall, average hardness measurements of nitrided regions was ~200VHN to ~500VHN higher than the Ti-6Al-4V material.

Table 4.8 Average micro-hardness values obtained from horizontal regions in the cross-section corresponding to images shown in Figure 4.23

	Average (VHN)	Standard Deviation
	496.3	17.8
	469.2	24.8
Nitride Layer	727.0	76.7
	536.2	24.4
	529.3	44.0
	484.5	38.1
	496.7	15.6
	485.8	25.3
	479.8	35.3
Nitride Layer	1049.2	241.3
	518.0	21.8
	544.7	19.1
	495.5	35.1

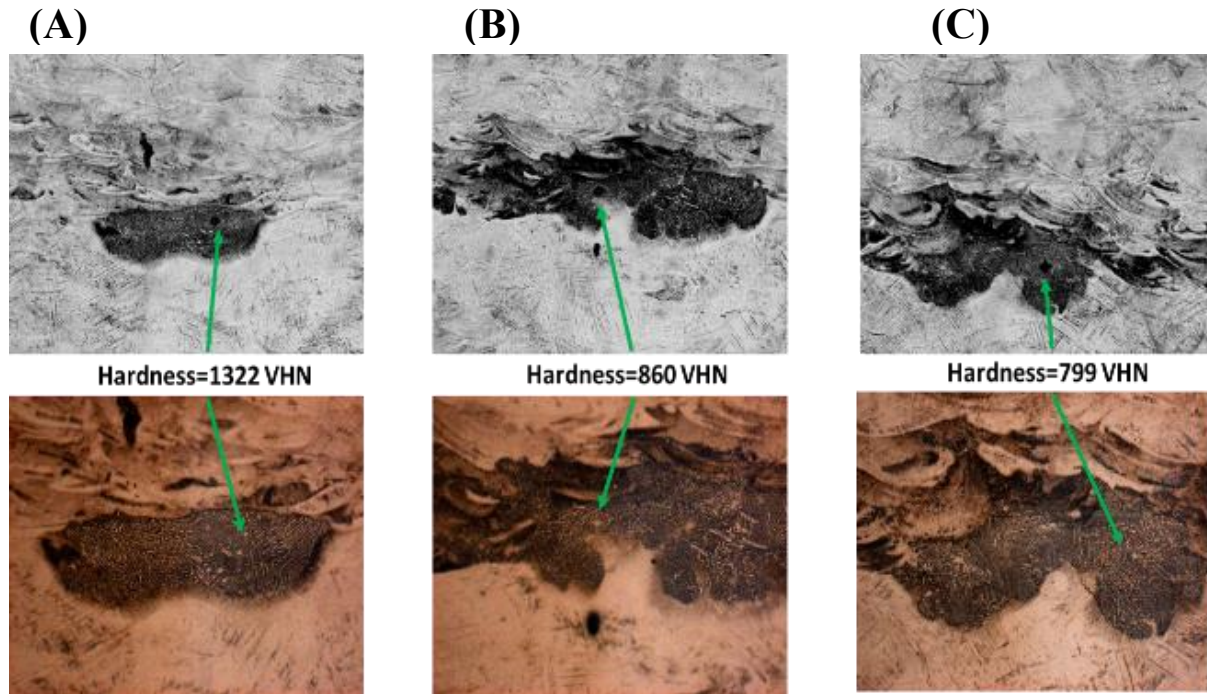


Figure 4.23 A) The highest micro-hardness value measured in the nitrided regions. B) A medium value measured in the nitrided regions. C) A lower hardness value measured in the nitrided region.

4.8 SANDWICH EXPERIMENT 2

The secondary sandwich experiment produced the same results as the initial sandwich experiment. No rotation of the scanning angle resulted in cracking in all samples. However, the experiment did prove useful in allowing the nitride layers to be seen before fabrication resumes. The nitride layers seen in Figure 4.24 (C) help support the results obtained from the initial sandwich experiment as only the continuous wave laser parameters produced an observable nitride layer. Cracking was observed on the outer surface of the samples and witness lines were observed in two regions along the sample's height where fabrication was paused and resumed as seen in Figure 4.24 (B).

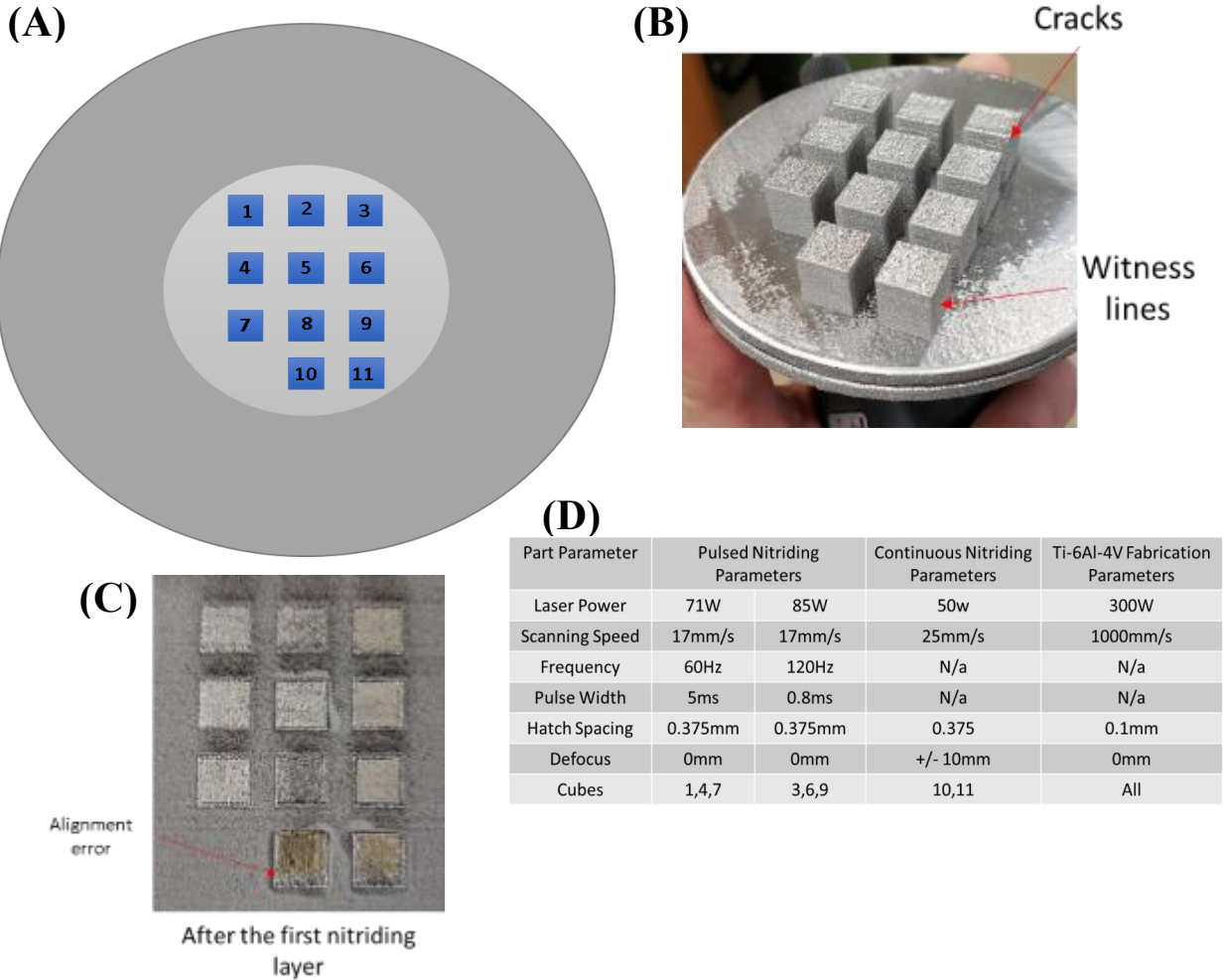


Figure 4.24 A) Displays the setup of the samples. B) The view of the outer defects immediately after fabrication. C) Top view taken post nitriding before the continuation of the fabrication process. D) Parameters used during the fabrication and nitriding.

4.9 Ti-6AL-4V/TiN PARAMETER REFINEMENT TEST

The cube surface test was performed in order to evaluate the laser nitriding parameters in more depth. Parameters were separated based off of how they were to be changed. Samples 1-5 utilized a constant laser power with changes to scanning speed and defocus, samples 6-9 maintained a constant laser power and scanning speed with changes only to defocus, and samples

10-16 maintained constant defocus while changing input power through the modification of laser power and/or scanning speed.

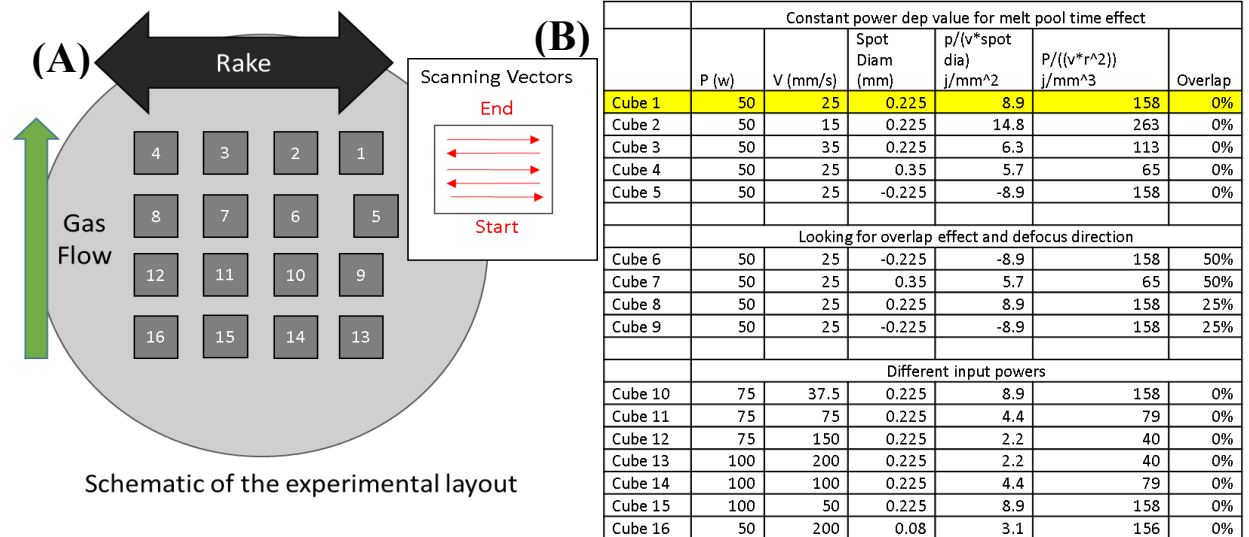


Figure 4.25 A) Depicts the setup utilized for the samples as well as the rake and gas flow directions. B) Demonstrates the laser parameter settings for all samples.

All samples showed the formation of a golden color on the top surface indicating the formation of titanium nitride. Cube numbers were engraved on the right side of each sample and are not flaws.

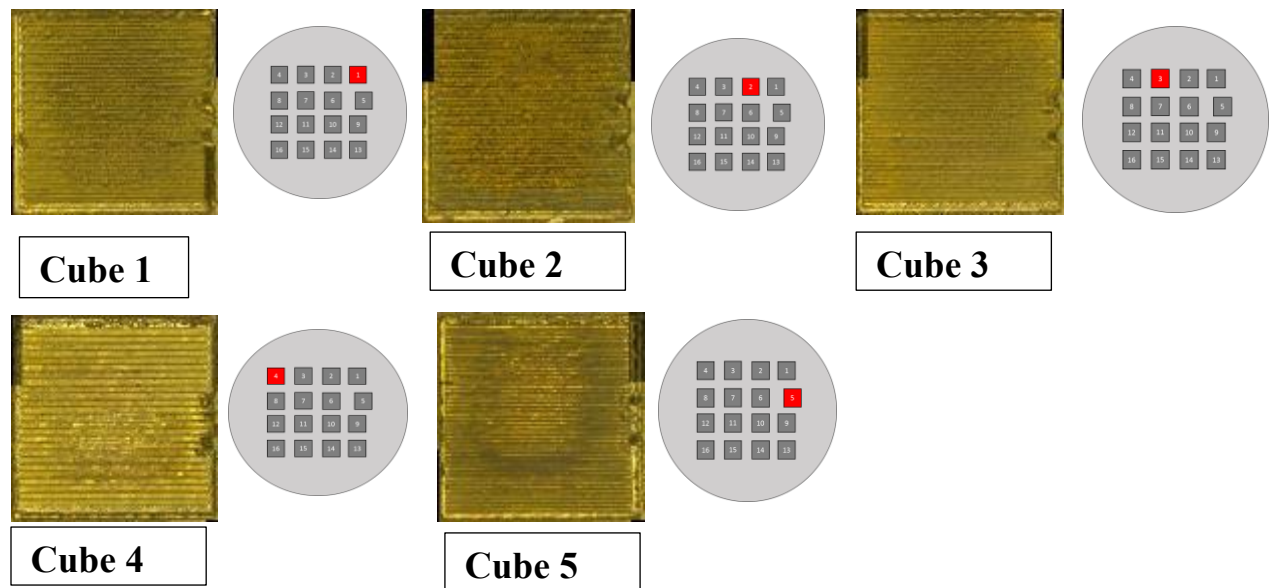


Figure 4.26 Samples maintained a constant laser power with varying scanning speeds and defocus levels.

Samples 1-5, all utilized constant laser power settings of 50W with changes to the scanning speed and defocus levels. For cubes 1-5, scanning speeds were 25mm/s, 15mm/s, 35mm/s, 25mm/s, and 25mm/s; with a 0% overlap for all parameters. The first set of samples in Figure 4.26, show mostly uniform nitrided surfaces. The varying scan speed changes in cubes 1, 2, and 3 show no major changes on the top surface except for a slight darkening in color transitioning from cube 3 as the lightest golden color to cube 1 and finally cube 2 as they got progressively darker. The darker colored surface corresponded to the slowest scan speed and the lightest gold color to the fastest scanning speed. Cubes 4 and 5 parameters saw a change in spot size with constant scan speed and defocus. Cube 4 showed some slight discoloration in the bottom half while cube 5 had dark regions in multiple locations creating a dark circular geometry.

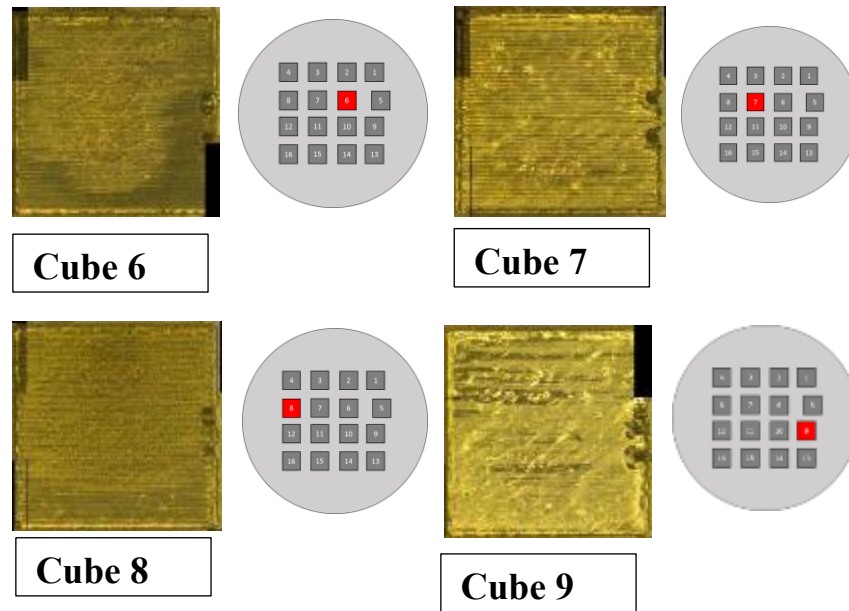


Figure 4.27 Samples maintained a constant power level and scanning speed with varying defocus causing variable overlap percentages.

The second set of samples cubes 6-9, seen in Figure 4.27, maintain constant laser power and scanning speeds at 50W and 25mm/s respectively, with varying defocus levels and changes to the overlap between laser scans. Cube 6 and 7 shared a 50% overlap while cubes 8 and 9 shared a 25% overlap. Cube 6 had a spot size of 0.225 under a negative defocus and showed the most inconsistent surface with a larger dark region on the bottom edge of the sample. Cube 7 had a spot size of 0.35mm from the use of a positive defocus value while not showing any large areas of discoloration. The differences can most noticeably be seen in the surface finish of the samples as Cube 8 and 9 shared a spot size of 0.225mm but used a positive and negative defocus respectively. Cube 9 showed a glossier surface finish while cube 8 demonstrated a matte finish with the upper half producing a rougher texture than its bottom stripe.

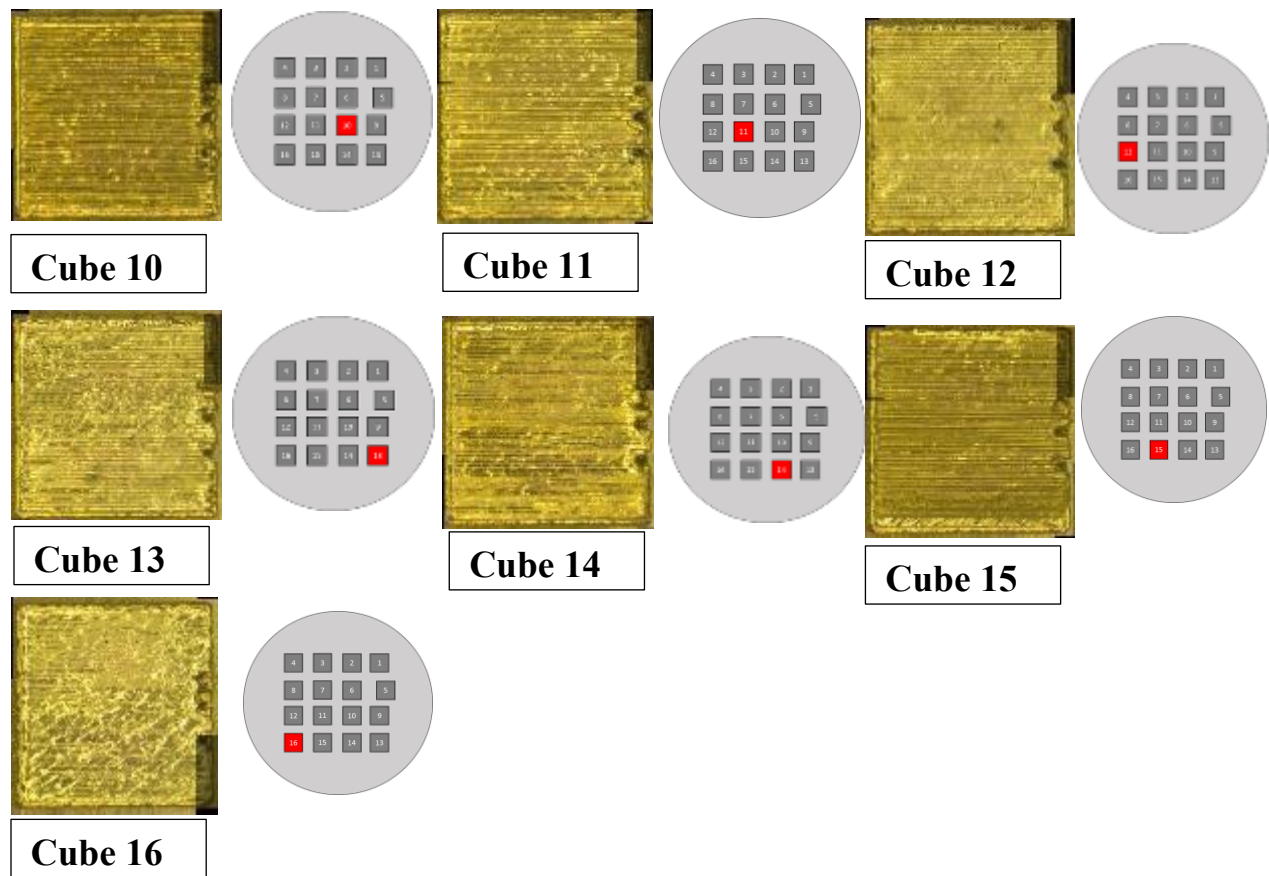


Figure 4.28 Samples contained varying laser power and scanning speed with consistent spot size and no overlap.

Parameters used constant spot diameters the last set of samples, cubes 10-16, seen in Figure 4.28 maintained the same defocus and no overlap value but greatly varied the input laser power and scanning speed the final set of samples presented in Figure 4.28, utilized no overlap value while varying laser power and scanning speed. Cubes 10-12 utilized the same laser power at 75 W with a consistent spot size of 0.225mm and increasing scans speed of 37.5mm/s, 75mm/s, and 150mm/s respectively. Cubes 13-15 also utilized consistent laser power but at 100W. These cubes shared a spot size of 0.225mm with decreasing laser scan speeds of 200mm/s, 100mm/s, and 50mm/s. Cube 16 used a completely different laser parameter set at 50W and 200mm/s. Gaps between scan lines can be seen on the bottom edge of the cubes. All samples show signs of nitriding proving there are

multiple parameter settings at which nitriding is possible. One noticeable observation with cubes 13, 14, and 15 is that as scanning speed decreases, there is an increase in dark regions of the sample surface. pattern that can be observed however is the darkening of the nitride between samples 10, 11, and 12. This observation holds true for cubes 13, 14, and 15.

CHAPTER 5: CONCLUSION

5.1 DISCUSSION

The nitriding results presented have shown that in-situ nitriding process is possible in an additive manufacturing environment. The nitriding results varied from material to material and is speculated to be affected by nitrogen concentration in the processing chamber, and the laser nitriding parameters such as laser power, scan speed, and spot size. Due to the nitriding process being a diffusion process, the gas concentration in which it is performed can affect the nitride quality. Low nitrogen levels in the processing chamber can lead to little or no nitrogen diffusion that may negatively affect the formation of TiN dendrites in the microstructure. Similarly, the laser parameters must provide sufficient thermal energy to allow for the successful diffusion into the substrate. Low levels of laser energy may cause minimal melting of the substrate causing for the formation of very thin nitride layers. Excessive laser energy however may cause excessive penetration into the substrate promoting the formation of cracking within the microstructure. The duration of which the substrate remains in its molten state is the time frame in which nitrogen is able to diffuse. Too little exposure can cause the formation of nitrogen rich Ti without the formation of any TiN dendrites and no substantial increase in material hardness nor a change in surface color.

The nitriding results yielded from the wrought Grade 2 substrates demonstrated the ability to produce nitrided layers and additional layers fabricated over its surface. The nitriding produced TiN layers with a thickness exceeding 50 μ m as can be seen in Figure 4.5 and Figure 4.7 but did show signs of minor cracking throughout the cross-section. The nitride layers produced exceed the thickness of nitride layers typically used for the production of TiN coated parts. Microhardness values measured from the TiN layers of the wrought Grade 2 substrates ranged from 1200-1800 VHN which is lower than the sourced hardness of value of TiN that can go up to as high as 3000

VHN (Ani Zhecheva, 2004). These lower hardness values may be attributed to way in which the TiN dendrites were formed during the nitriding process. The conditions under which TiN is formed is different as laser nitriding makes use of extremely short time span when compared to nitriding methods such as gas nitriding which can occur over the course of hours may explain the difference in material hardness. MW laser parameters on Ti-6Al-4V substrates allowed for the importance of the overlap and hatch spacing values to be better observed along with laser parameters previously studied. The nitriding performed showed different levels of penetration and melt pool geometry through several iterations of experiments. Many of the images observed of melt pool geometry were dependent on the location at which the sample was sectioned, however the geometries followed the shape depicted in Figure 2.2 The kinetics into why there was changes in the melt pool width within the same laser scan are unknown, however it was seen that wider melt pools provided a more consistent nitriding surface and did not produce gaps of Ti-6Al-4V between scans such as in Figure 4.9 (A).

Fabrication laser parameters were modified from initial parameter sets to produce Ti-6Al-4V substrates with less residual stress. Initial attempts caused substantial internal and external cracking throughout the samples due to flawed laser scanning angle settings. Increased laser power from 300W to 330W, as well as a rotating beam angle of 67° produced higher quality Ti-6Al-4V fabricated substrates. The results from surface nitriding performed on fabricated Ti-6Al-4V demonstrated the CW laser parameters had better diffusion of nitrogen into the substrate due to the formation of dendrites that were absent in the majority of the MW parameter samples as seen in Figures 4.12 and Figure 4.13 The shapes in the melt pools however varied throughout the cross sections as can be seen in Figure 4.16 (B) and (C). These shapes directly reflect the phenomena in the shape formation of melt pools based off the flow of eddy currents (A. Arora, 2008). Similar

melt pool geometries formed in melt pools of the pulsed parameters (Figures 4.14-Figure 4.16). The swirled melt pool in Figure 4.15 in particular has a more detailed view of the eddy flow current within the melt pool during its molten stage. It is speculated that the solidification rate occurred in an extremely short amount of time limiting diffusion and producing a swirled matrix of titanium and nitrogen exposed titanium (A. Arora, 2008). The penetration of the melt pools compiled from all the surface nitrided samples demonstrated a correlation between the melt pool depth and defocus value. The focused beam with a defocus value of 0mm produced an average penetration depth of $\sim 175\mu\text{m}$ while defocus values of $\pm 10\text{mm}$ only penetrated to a depth of $\sim 51\mu\text{m}$ and $\sim 85\mu\text{m}$. Comparing the largest defocus melt pools CW laser parameters penetrated $\sim 3\mu\text{m}$ deeper for +10mm defocus, and $\sim 21\mu\text{m}$ deeper for -10mm defocus when compared to the MW laser settings.

Initial sandwich build contained severe internal and external cracking due to residual thermal stresses caused by the fabrication process. The undistributed thermal stress was caused by the 180° rotation angle of the laser beam. Locations of increased thermal stress such as nitrided regions were more prone to cracking. Figure 4.22. helps to visualize this demonstrating the crack propagation initializing at the nitrided region. The nitrided regions in the sandwich substrate depicted dendrites, particularly with the CW laser parameter samples, but showed greater melt pool variation when compared to the melt pools created from identical parameters on a surface nitriding setup. Microhardness measurements performed on nitrided regions ranged from 600VHN to 1300VHN lower than expected TiN values (Chi-Wai Chan S. L.-H.-C., 2015) but did show an increase compared to the surrounding Ti-6Al-4V substrate hardness of $\sim 500\text{VHN}$. The hardness values taken in the nitrided regions on the lower nitride layer were higher than those taken from the upper nitride layer by $\sim 300\text{VHN}$. This change may be attributed

to different levels of nitrogen content in the fabrication chamber or different temperatures of the substrate at the time of nitriding.

The cube surface test, tested small changes in laser parameters such as defocus, overlap, scan speed and laser power and how each type of change affected the nitride layer. The change of overlap in laser scanning had an impact on the surface finish of nitrided structures as was shown in Figure 4.27, while visual aspects such as the color/darkness of the nitrided area were more dependent on the scan speed. Changes in scan speed, specifically in the decrease of the scanning speed caused a darkening effect on nitrided regions as seen in Figure 4.26 Further microstructural analysis and microhardness testing is required to determine the effects caused to the nitride quality by the modification in small increments of such parameters. Regardless of parameter set, it has been shown that a combination of slower scan speeds as well as higher laser power increase the penetration of nitride into the substrate however the increased input power also increases the likelihood of cracking. Experimentation performed utilizing MW laser parameters demonstrated a more consistent melt pool geometry and penetration depth compared to CW but did not have as efficient nitriding seen in minimal presence of dendrites.

5.2 CONCLUSION

Metal matrix composites of Ti and Ti-6Al-4V base substrates with internal TiN structures were successfully fabricated. The laser parameters utilized during the nitriding process have a significant impact on the formation of dendrites in the microstructure with higher energy levels producing thicker and harder TiN layers, that also contained more melt pool deformation and cracking. Between laser parameters, CW laser sets produced more dendrites within the nitrided region microstructure. MW laser parameter sets produced a more consistent melt pool geometry; however, the short processing time did not allow for enough nitrogen to diffuse during nitriding leading to very little or no dendrite formation as well as lower hardness values than other parameter

sets. The re-melting of additional layers atop nitrided regions has demonstrated to interfere with nitride layers below as regions surrounding TiN layers show an increase in hardness though to be caused by diffusion of nitrogen from the TiN layer into the surrounding region. Regions of the substrate located directly below nitrided regions demonstrated a minor increase of hardness, this may be from nitrogen diffusion that penetrated through the nitride layer, formation of alpha prime TiN, or nitrogen was diffused from the nitrided region into the surrounding substrate caused by the fabrication.

5.3 FUTURE WORK

Future work into the integration of selective nitriding and LPBF should focus on laser parameter refinement to combine nitrided regions within substrates while maintaining the physical properties in TiN coatings. The current nitriding process uses vast quantities of nitrogen gas and must be adapted to a process in which the wasted gas is greatly reduced. An open source LPBF system is of great benefit in nitriding as it allows for the manipulation of a larger variety of parameters, settings, and processes to be adjusted, however a smaller fabrication chamber would help increase the speed at which the process is accomplished. If fabrication of Ti-6Al-4V substrates can be achieved in a nitrogen or nitrogen mixed environment without high levels of nitrogen diffusion, it would allow for a much more effective and efficient process and may prove the most ideal method. More testing using CW parameters with high laser power settings with higher laser scanning speeds may also be beneficial to compare to that CW that utilized low values for laser power and scanning speed.

REFERENCES

- A R Nassar, R. A. (2012). Investigations of laser-sustained plasma and its role in laser nitriding of titanium. *Journal of Physics D: Applied Physics*, 10.
- A Schultz, D. M. (2009). Partial Laser and gas nitriding of titanium components. *HTM Journal of Heat Treatment and Materials*, 8.
- A. Arora, G. R. (2008). Unusual wavy weld pool boundary from dimensional analysis. *Scripta Materialia*, 4.
- Abboud, J. (2012). Effect of processing parameters on titanium nitrided surface layers produced by laser gas nitriding. *Surface & Coatings Technology*, 11.
- Ani Zhecheva, W. S. (2004). Enhancing the microstructure and properties of titanium alloys through nitriding and other surface engineering methods. *Surface & Coatings Technology*, 16.
- B.S. Yilbas, C. K. (2006). Co2 laser gas assisted nitriding of Ti-6Al-4V alloy. *Applied Surface Science*, 8.
- Chi-Wai Chan, S. L. (2016). Fiber laser nitriding of titanium and its alloy in open atmosphere for orthopaedic implant applications: Investigations on surface quality, microstructure and tribological properties. *Surface & Coatings Technology*, 13.
- Chi-Wai Chan, S. L.-H.-C. (2015). Enhancement of wear and corrosion resistance of beta titanium alloy by laser gas alloying with nitrogen. *Applied Surface Science*, 11.
- Deepak, J. (2015). A Review on Surface Engineering Of Ti6Al4V Titanium Alloy Using Gas and Laser Nitriding Techniques. *Trans Tech Publications*, 9.
- Direct Metal Laser Sintering*. (2012, 1 15). Retrieved from Custompart.net: <http://www.customnet.com/wu/direct-metal-laser-sintering>
- E. Gyorgy, A. P. (2002). Surface nitridation of titanium by pulsed Nd:YAG laser irradiation. *Applied Surface Science*, 5.
- Edson Costa Santos, M. M. (2006). Laser gas nitriding of pure titanium using CW and pulsed Nd:YAG lasers. *Surface & Coatings Technology*, 7.
- Filip, R. (2008). Laser nitriding of the surface layer of Ti6Al4V titanium alloy. *Archives of Materials Science and Engineering*, 4.
- H.C. Man, M. B. (2011). Laser diffusion nitriding of Ti-6Al-4V for improving hardness and wear resistance. *Applied Surface Science*, 6.
- Kaufui V. Wong, A. H. (2012). A Review of Additive Manufacturing. *Hindawi*, 11.
- L. Xue, M. U. (2007). Laser Gas Nitriding of Ti-6Al-4V Alloy. *Materials and Manufacturing Processes*, 20.
- Lisiecki, A. (2015). Titanium Matrix Composite Ti/TiN Produced by Diode Laser Gas Nitriding. *MDPI*, 16.
- Luther M. Gammon, R. D. (2004). Metallography and Microstructures of Titanium and Its Alloys. In G. F. Vander Voort, *Metallography and Microstructures* (p. 21). ASM International.
- M Raaif, F. M.-H. (2008). Co2 laser nitriding of titanium. *Journal of Physics: Applied Physics*, 8.
- Naofumi Ohutsu, K. K. (2010). Comparison of surface films formed on titanium by pulsed Nd:YAG laser irradiation at different powers and wavelengths in nitrogen atmosphere. *Applied Surface Science*, 4.

- Pye, D. (2003). An introduction to nitriding. In D. Pye, *Practical Nitriding and Ferritic Nitrocarburizing* (p. 13). Ohio: ASM International.
- S. Fare, N. L. (2012). Properties of nitrided layers formed during plasma nitriding of commercially pure Ti and Ti-64 alloy. *Surface & Coatings Technology*, 6.
- Shunyu Liu, Y. C. (2019). Additive Manufacturing of Ti6Al4V alloy: A review. *Materials Design*, 23.
- Udroiu, R. (2015). Powder Bed Additive Manufacturing Systems and its Applications. *Academic journal of manufacturing engineering*, 9.
- Valmik Bhavar, P. K. (2016). A Review on Powder Bed Fusion Technology of Metal Additive Manufacturing. *Semantic Scholar*, 8.
- Vojislav Petrovic, J. V. (2012). Additive Manufacturing Solutions for Improving Medical Implants. *IntechOpen*, 37.
- Wei Quan Toh, P. W. (2016). Microstructure and Wear Properties of Electron Beam Melted Ti-6Al-4V Parts: A Comparison Study against As-Cast Form. *MDPI*, 13.
- Yang, M. (2012). Nitriding-fundamentals, modeling and process optimization. 139.

VITA

Andres Gerardo Navarro born December 30, 1995 and is the son of Mr. Raul G. Navarro and Mrs. Yvette Navarro. Andres obtained his high school diploma in May of 2014 from Cap. John L. Chapin High School in El Paso Texas. He obtained his Bachelor of Science Degree in Mechanical Engineering at the University of Texas at El Paso in December of 2017. While pursuing his Master of Science Degree, Andres completed a certification in Additive Manufacturing provided by the W.M. KECK Center for 3D Innovation. Andres conducted research at the W.M. KECK Center and presented his research at the SETS southwest conference in the spring of 2019.

Permanent address: 6736 Marble Canyon
El Paso, TX, 79912

This thesis/dissertation was typed by Andres Gerardo Navarro